Journal of Medicinal Chemistry

Discovery of nanomolar desmuramylpeptide agonists of the innate immune receptor nucleotide-binding oligomerization domain-containing protein 2 (NOD2) possessing immunostimulatory properties

Martina Gobec, Tihomir Tomaši#, Adela Štimac, Ruža Frkanec, Jurij Trontelj, Marko Anderluh, Irena Mlinaric-Rascan, and Žiga Jakopin

J. Med. Chem., **Just Accepted Manuscript** • DOI: 10.1021/acs.jmedchem.7b01052 • Publication Date (Web): 15 Mar 2018

Discovery of nanomolar desmuramylpeptide agonists of the innate immune receptor nucleotide-binding oligomerization domain-containing protein 2 (NOD2) possessing immunostimulatory properties

Martina Gobec[1], Tihomir Tomašič[1], Adela Štimac[2], Ruža Frkanec[2], Jurij Trontelj[1], Marko Anderluh[1], Irena Mlinarič-Raščan[1] and Žiga Jakopin[1,]*

[1]Faculty of Pharmacy, University of Ljubljana, Aškerčeva 7, SI – 1000 Ljubljana, Slovenia.

[2]University of Zagreb, Centre for Research and Knowledge Transfer in Biotechnology, Rockefellerova 10, 10000 Zagreb, Croatia.

*Corresponding author:
Žiga Jakopin
Phone: +386 1 4769 646
Fax: + 386 1 4258 031
E-mail address: ziga.jakopin@ffa.uni-lj.si

Abstract:

Muramyl dipeptide (MDP), a fragment of bacterial peptidoglycan, has long been known as the smallest fragment possessing adjuvant activity, on the basis of its agonistic action on the nucleotide-binding oligomerization domain-containing protein 2 (NOD2). There is a pressing need for novel adjuvants and NOD2 agonists provide an untapped source of potential candidates. Here, we report the design, synthesis and characterization of a series of novel acyl tripeptides. A pivotal structural element for molecular recognition by NOD2 has been identified, culminating in the discovery of compound **9**, the most potent desmuramylpeptide NOD2 agonist to date. Compound **9** augmented pro-inflammatory cytokine release from human peripheral blood mononuclear cells in synergy with lipopolysaccharide. Furthermore, it was able to induce ovalbumin-specific IgG titers in a mouse model of adjuvancy. These findings provide deeper insights into the structural requirements of desmuramylpeptides for NOD2-activation and highlight the potential use of NOD2 agonists as adjuvants for vaccines.

Keywords:

Muramyl dipeptide, immunomodulator, desmuramylpeptide, NOD2 agonist, immunostimulant, adjuvant

1. INTRODUCTION

Innate immunity, once assumed to be the redundant remnant of an ancient antimicrobial system, is in fact the cornerstone of the body's ability to combat infection.[1] Pattern recognition receptors (PRRs) comprise a constellation of evolutionarily conserved immune sensors that possess the ability, not only to sense invading pathogens via the detection of their specific molecular signatures, but also to orchestrate the initial defense response as part of the innate immune process.[1] Nucleotide-binding oligomerization domain-containing protein 2 (NOD2), that belongs to a major cytosolic class of PRRs, the NOD-like receptors (NLR), is of utmost importance since it has an important task within the innate immune response.[2] It is predominantly expressed in immune cells and, to a lesser degree, in Paneth cells and certain epithelial cells.[2,3] The structure of NOD2 protein is assembled from the following structural units: two caspase activation and recruitment domains (CARDs), a nucleotide-binding oligomerization domain (NOD) and multiple leucine-rich repeats (LRRs). It has been suggested that it typically exists in an autoinhibited state.[4]

Muramyl dipeptide (MDP), a conserved constituent of the cell wall of the majority of types of bacteria, is the smallest structural subunit of bacterial peptidoglycan capable of eliciting NOD2 activation[5,6]; direct contact between MDP and NOD2 has recently been proven by both biophysical and biochemical assays.[7,8] On recognition of MDP, NOD2 undergoes self-oligomerization and activates the serine-threonine kinase receptor-interacting protein 2 (RIP2). Subsequently, the nuclear factor κB (NF-κB) and mitogen-activated protein kinase (MAPK) signaling pathways are initiated, resulting in the production of cytokines, certain antimicrobial peptides and induction of additional processes, which characterize a proinflammatory/antimicrobial response. [3,7,9] Of note, a number of regulatory proteins closely control the downstream signaling pathways underlying NOD2 activation.[9]

Activation of NOD2 itself is sufficient to shape adaptive immune responses[10,11] but, more importantly, NOD2 agonist synergistically augments the adjuvant capacity of other PRR ligands such as Toll-like receptor (TLR) ligands. This NLR-TLR crosstalk has been proved to be essential for adaptive immunity and underlines the importance of NLRs.[12-15] Interestingly, in spite of innate immunity not being known to possess memory, NOD2 ligands have been shown to induce epigenetic reprogramming of monocytes, resulting in nonspecific protection against reinfection; this phenomenon has been termed "trained immunity".[16,17] Recently gained insight into the crosstalk between innate and adaptive immune responses is of significant clinical importance and has opened up new avenues for development of novel vaccines.[18] Curently, only four adjuvants are approved for human vaccines in the US and Europe. Although MDP was long ago identified as the smallest component underlying the efficacy of Freund's complete adjuvant, thus opening up a new era in immunology, it has proved to be too pyrogenic for clinical application, while it also suffers from rapid elimination.[19,20] Therefore, MDP has been limited to veterinary vaccines.[20] Besides their adjuvant properties, NOD2 agonists have been shown to possess indirect antimicrobial properties as well as the ability to act synergistically in combination with antibiotics and to stimulate the non-specific resistance against infections and tumors.[18,21,22]

Recent decades have witnessed the discovery of diverse nonpyrogenic MDP analogs, either chemically modified MDP derivatives or conjugated with carriers, with preserved adjuvant/immunostimulatory activity.[23-32] Certain lipophilic derivatives of MDP have exhibited stronger adjuvant activity than that of the parent structure, showing that MDP can be tailored to increase the adjuvant activity.[20, 30, 31] Thus mifamurtide has been tested as part of an influenza vaccine in a number of clinical trials.[21]

The term "desmuramylpeptides" refers to MDP derivatives lacking the sugar *N*-acetylmuramyl moiety (Mur*N*Ac). It has been shown unequivocally that the presence of Mur*N*Ac is not mandatory for NOD2 recognition, as evidenced by recently developed desmuramylpeptides possessing NOD2 agonistic activity.[24,25,33,34] Here, we describe the design, synthesis and characterizarion of a series of novel acyl tripeptides as a continuation of our efforts to generate desmuramylpeptides with potent NOD2 agonistic activity. The NOD2-dependent NF-κB activation capacity of the synthesized library of fourth generation desmuramylpeptides has been determined on HEK293 cells overexpressing the NOD2 gene. The pivotal structural elements of acyl tripeptides for molecular recognition by NOD2 were identified. Compound **9**, in which the carbohydrate moiety was replaced by a *trans*-feruloyl moiety, has been identified as the strongest desmuramylpeptide NOD2 agonist to date, being twice as potent as MDP. Its immunostimulatory properties have been determined in *in vitro* experiments that revealed the capacity of **9** to augment pro-inflammatory cytokine release from human peripheral blood mononuclear cells (PBMC), by itself and in synergy with lipopolysaccharide (LPS). Furthermore, when co-administered subcutaneously with the model antigen, ovalbumin (OVA), it induced OVA-specific IgG titers in a mouse model of adjuvancy. These findings provide deeper insights into the structural requirements of desmuramylpeptides for NOD2-activation and point out the potential utility of NOD2 agonists as adjuvants for vaccines.

2. RESULTS AND DISCUSSION

2.1 Design

The SLC15 family of peptide transporters, outer membrane vesicles and endocytosis have all been suggested as a potential entry route of MDP into the cytoplasm,[35-38] while desmuramylpeptides were shown to cross the membrane via passive absorption.[39] In

accordance with this, the introduction of lipophilic groups into the structures of NOD agonists, as well as the use of lipophilic delivery carrier systems, strongly enhanced the cellular immunity and strikingly increased the adjuvant activity of compounds, further reinforcing this suggestion.[31,40,41] Similarly, previous studies of the structure-activity relationships (SAR) of MDP derivatives established that introduction of a lipophilic moiety into MDP can increase its adjuvant activity.[42-44] Although the molecular nature of the interaction between MDP and NOD2 is not known, in our previous research, cinnamoyl-Gly (*i.e.* compound **II**) and 6-Ph-indole-Gly (*i.e.* compound **I**) moieties were highlighted as appropriate surrogates for the Mur*N*Ac group. Leads **I** and **II** were identified as effective NOD2 agonists and were selected for further optimisation (Fig. 1).[24,25,34] The structural requirements thus elucidated for NOD2 agonist activity also include the presence of ethyl ester groups at the D-Glu moiety.

Here, we explored the chemical space of our leads **I** and **II** (shown in Fig. 1) and investigated how modifications of the amino acid type and the acyl moiety affect their NOD2 agonist activity. The underlying principle that guided our design was the previously reported promising immunostimulatory effect of lipophilic derivatives. In the light of this, we decided to modify the tripeptide and carbohydrate moiety so that the analogs bear the features of leads **I** and **II**, while differing from each other in subtle substitutions. The first group of modifications involved replacement of the L-Ala residue with its more lipophilic counterparts, L-Val and L-Phe, since only limited variations of the essential L-Ala-D-*iso*Gln pharmacophore are allowed.[42,43] Also, a previous study has suggested that, by designing MDP derivatives harboring L-Val, it should be posssible to decouple the inflammation-inducing capacity from the ability to induce adaptive immunity.[42] The second group of modifications includes replacement of the aforementioned acyl moieties by a careful selection of their closely related

mimetics. As the analogs needed to be synthetically accessible, we focused more intensively on modifications of the cinnamoyl rather than the 6-phenylindole fragment. Unsubstituted and substituted cinnamoyl moieties are present in many natural products and drugs. The feruloyl (4-hydroxy-3-methoxycinnamoyl) moiety, for example, is considered to be a privileged fragment and has found application as a component of the drug cyclovalone.[45] In addition, the cyclopropyl ring system has been introduced into the cinnamoyl moieties as a bioisosteric replacement of the alkene bond. It is woth noting that cyclopropane has increasingly been featured in a wide array of drugs with the aim of preventing the isomerization of the *E*/*Z* alkene bond and/or facilitating the projection of the attached groups in a desirable *trans*-geometry.[46] Finally, minor modifications were also introduced into the D-Glu residue of the tripeptides by equipping this moiety with rigid mimetics. The previously reported conformationally constrained mimetics of D-glutamic acid[47] were incorporated into the structure of **9**, used as the starting point, with the aim of potentiating its NOD2-agonistic activity. This optimization approach has been well-known among medicinal chemists for decades. These combined efforts afforded several novel desmuramyldipeptides which were tested for their NOD2-agonist properties on the commercially available HEK-Blue NOD2 cell line.

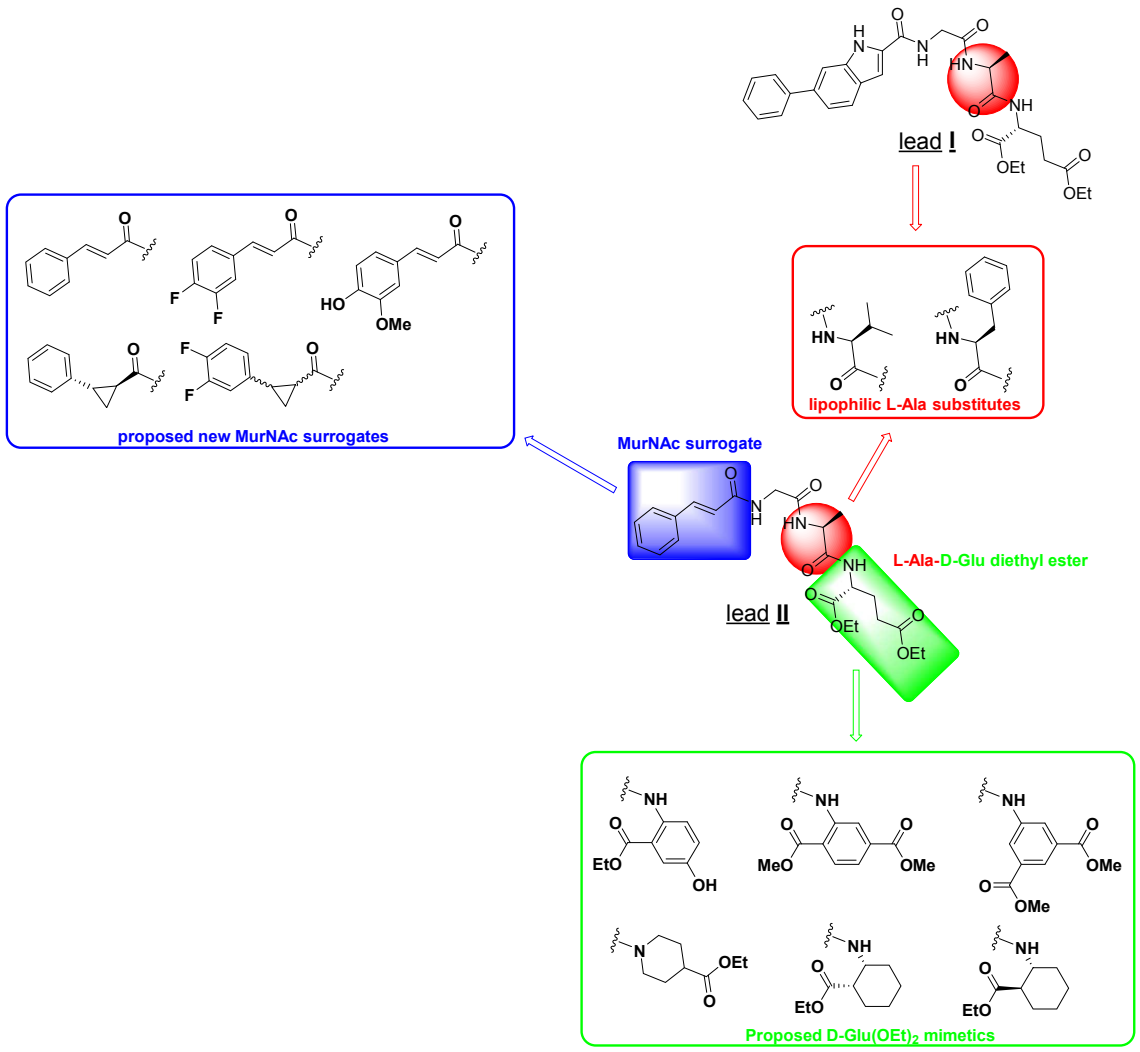

Figure 1. Design of acylated tripeptide analogs and structural modifications of leads **I** and **II**.

2.2 Chemistry

Preparation of tripeptides was guided by the desire to establish a reproducible and convenient route suitable for multigram production. Thus, a four step synthesis of the key intermediates Boc-Gly-L-Val-D-Glu(OEt)$_2$ (**3a**) and Boc-Gly-L-Phe-D-Glu(OEt)$_2$ (**3b**) was executed as shown in Scheme 1. The starting D-glutamic acid was first esterified via acid-catalyzed esterification, using $SOCl_2$ in ethanol, to yield the corresponding diethyl ester **1a**. The crude diethyl ester was then coupled with Boc-L-Val or Boc-L-Phe, using dicyclohexylcarbodiimide (DCC)/1-hydroxybenzotriazole (HOBt) methodology, thus giving the corresponding

dipeptides Boc-L-valyl-D-glutamic acid diethyl ester (**2a**) and Boc-L-phenylalanyl-D-glutamic acid diethyl ester (**2b**). The Boc-protecting group was then removed from **2a**/**2b** under acidolytic conditions using trifluoroacetic acid (TFA), followed instantly by coupling with Boc-Gly, thus affording the Boc-protected tripeptides Boc-Gly-L-Val-D-Glu(OEt)$_2$ (**3a**) and Boc-Gly-L-Phe-D-Glu(OEt)$_2$ (**3b**). The Boc-protecting group was removed from tripeptides **3a** and **3b**, using TFA, giving the corresponding trifluoroacetate salts of the tripeptides. Having prepared intermediates that enable acylation of the free amino group of Gly at a late-stage , we generated several compounds with diverse functionalities in order to ascertain how minimal modifications of the cinnamoyl moiety affect the NOD2-agonistic activities of the compounds. By coupling of the commercially available acids with the key intermediates **3a** and **3b**, using standard 1-ethyl-3-(3-dimethylaminopropyl)carbodiimide (EDC)/HOBt coupling methodology, corresponding *N*-acyl Gly-L-Val-D-Glu(OEt)$_2$ analogs **4-9** and *N*-acyl Gly-L-Phe-D-Glu(OEt)$_2$ analogs **10-15** (see Scheme 1) were afforded.

Scheme 1.[a] Synthesis of acylated tripeptide analogs.

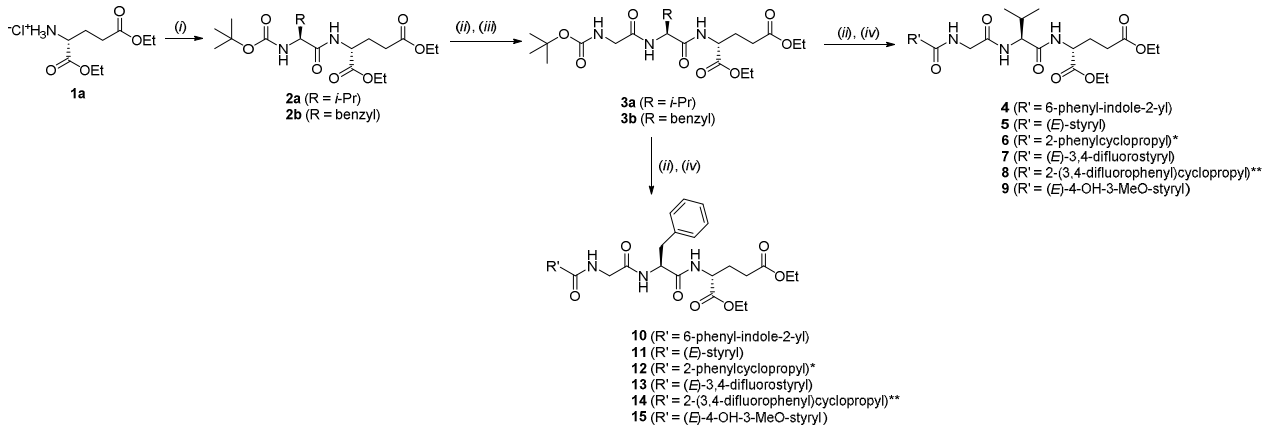

[a] Reagents and conditions: (*i*) Boc-L-Val or Boc-L-Phe, DCC, HOBt, DIPEA, DMAP, EtOAc; (*ii*) TFA/CH_2Cl_2 (1:5); (*iii*) Boc-Gly, DCC, HOBt, DIPEA, DMAP, EtOAc; (*iv*) R'COOH, EDC, HOBt, DIPEA, DMAP, DMF. * a mixture of two diastereomers; ** a mixture of four diastereomers.

Similarly, an L-Ala carrying congener of **9**, compound **16**, was prepared by coupling *trans*-ferulic acid with Boc-Gly-L-Ala-D-Glu(OEt)$_2$ prepared as described [34]. Further, compound **9** was converted to its free acid analog **17** via alkaline hydrolysis (Scheme 2).

Scheme 2.[a] Synthesis of derivatives of compound **9**.

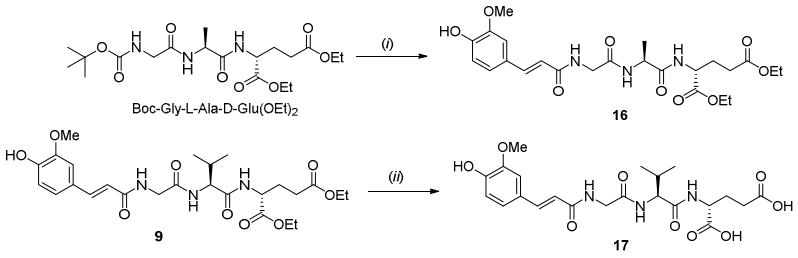

[a]Reagents and conditions: (*i*) *trans*-ferulic acid, EDC, HOBt, DIPEA, DMAP, DMF; (*ii*) 1M NaOH, EtOH, rt.

It has been reported that only minuscule variations of the second amino acid of the essential L-Ala-D-Glu moiety are allowed.[42,43] In order to determine how the incorporation of rigidified D-Glu mimetics affects the NOD2-agonistic activity, derivatives harboring modified D-Glu moiety were prepared by introducing previously reported constrained mimetics of D-glutamic acid[47] into the structure of compound **9** (Scheme 3). The glycine was first was first esterified via acid-catalyzed esterification, using $SOCl_2$ in ethanol, to yield the corresponding ethyl ester **1c**. The crude ester was then coupled with *trans*-ferulic acid, using EDC/HOBt methodology, affording the corresponding *N*-feruloyl derivative **18.** In the succeeding synthetic step, the ethyl ester was hydrolyzed under alkaline conditions, furnishing the free acid **19** which was coupled with HCl×L-Val-OEt (**1b**) to generate *N*-feruloyl dipeptide **20**. On alkaline hydrolysis of the latter, the intermediate free acid **21** was coupled with the commercially available amines using the established EDC/HOBt procedure, resulting in the desired rigidified mimetics of **9**, the compounds **22-24** (Scheme 3). Finally in order to investigate in what

manner the forced planarity − a direct consequence of the introduced aromatic ring − affects NOD2 recognition, *N*-feruloyl glycine **19** was also linked to aromatic mimetics of the L-Val-D-Glu dipeptide **25b**, **26b** and **27b** (prepared as described in Supporting Information) affording compounds **28-30**.

Scheme 3.[a] Exploration of the chemical space of D-glutamic acid.

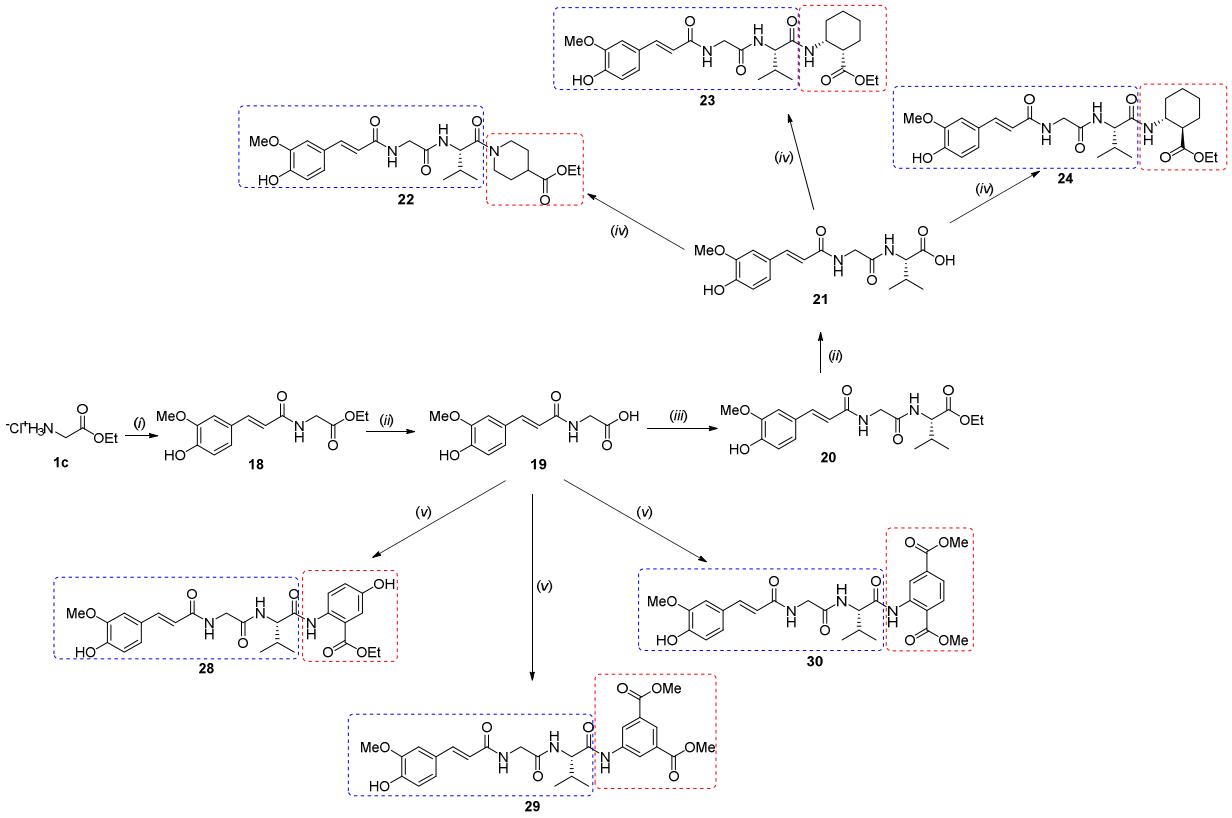

[a]Reagents and conditions: (*i*) *trans*-ferulic acid, EDC, HOBt, DIPEA, DMAP, DMF; (*ii*) 1M NaOH, EtOH, rt; (*iii*) **1b**, EDC, HOBt, DIPEA, DMAP, DMF; (*iv*) ethyl isonipecotate or ethyl (1*R*,2*S*)-2-aminocyclohexane-1-carboxylate or ethyl (1*S*,2*S*)-2-aminocyclohexane-1-carboxylate, EDC, HOBt, DIPEA, DMAP, DMF; (*v*) **25b** or **26b** or **27b**, EDC, HOBt, DIPEA, DMAP, DMF. Constrained mimetics of D-glutamic acid are highlighted in dashed red rectangles. Core structure of **9** is highlighted in dashed blue rectangles.

2.3 Biological studies

2.3.1 Evaluation of the cytotoxicity of the synthesized compounds

The cytotoxic potential of MDP and the novel desmuramylpeptides was first established by measuring the proliferation rates of HEK-Blue NOD2 cells treated with these compounds, using the standard metabolic activity assay. Cells were treated for 18 h with MDP and desmuramylpeptides at 20 μM concentration and their measured metabolic activities compared with that of the untreated control. The compounds proved to be non-cytotoxic to HEK-Blue NOD2 cells, since none of the residual metabolic activities were less than 80% at the tested concentration (Fig. S12).

2.3.2 Evaluation of NOD2-agonistic activity of the synthesized compounds

The ability of the synthesized desmuramylpeptides to activate NOD2 at the cell level was investigated employing a validated, commercially available HEK-Blue NOD2-dependent NF-κB-inducible SEAP (secreted embryonic alkaline phosphatase) reporter gene assay. NOD2 agonistic activity of a compound is directly related to the elicited NF-κB transcriptional activity and, in turn, the production of SEAP. HEK-Blue NOD2 cells were treated with desmuramylpeptides, and with MDP as the reference compound, for 18 h at 2 or 20 μM. The results were normalized to that of the untreated control (NT). Since all tested compounds initially exhibited maximal NOD2 activation at 20 μM (data not shown), the biological evaluation was repeated at the 10-fold lower concentration of 2 μM (Table S1). Of the 20 synthesized MDP-derived compounds, most belong to two parallel series of acyl tripeptides harboring modifications at the second amino acid and carrying slightly different acyl moieties. The ability of the synthesized acyl tripeptides **4** to **15** (the L-Val and the L-Phe series), with MDP as reference compound, to activate NOD2 at the level of the cell led to several interesting observations (Fig. 2). The majority of the compounds feature a cinnamoyl

structural motif, previously employed successfully in the preparation of lead **II**[34] and, surprisingly, in the recently disclosed MDP-derived NOD2 antagonists[48,49a] and dual NOD1/NOD2 antagonists revealed in a paper by Wang et al.[49b] The SAR analysis offered some explanation on how slight structural variations of the cinnamoyl moiety linked to the glycine amino group affect NOD2 activation, reflected by NF-κB transcriptional activity, with respect to untreated cells (1.0-fold) and MDP (5.6-fold NOD2 activation). It has been suggested that the 6-phenylindole fragment, as a surrogate of Mur*N*Ac, is a pivotal structural element for NOD2 recognition, as evidenced by our lead **I**.[34] Surprisingly, the 6-phenylindole-incorporating compound **4** was in fact a weaker NOD2 activator (3.9-fold) than all the cinnamoyl moiety-bearing analogs. All the tested variations of the substituted cinnamoyl derivatives were tolerated. Introduction of two fluorine atoms on the phenyl ring of **5** (5.7-fold), yielding the 3,4-difluorosubstituted **7** (5.6-fold), did not enhance the activity of the parent compound. Analogously, the 3-methoxy-4-hydroxy substituted derivative **9** proved to be as strong as the unsubstituted derivative **5**, with a 5.6-fold NOD2 activation. Cyclopropanation of the alkene moieties of **5** and **7** resulted in the corresponding cyclopropane-carrying derivatives **6** and **8** with NOD2 agonist activities of 4.4-fold and 5.8-fold. The minor drop in NOD2 activation capacity, as compared to that of the parent compound, is probably a result of the different spatial orientations of the diastereomers composing **6**. A similar trend was observed with the L-Phe series. The 3,4-difluorosubstituted **13** (5.4-fold) and the 3-methoxy-4-hydroxy **15** (5.7-fold) exhibited activities comparable to that of **11** (5.3-fold), harboring the unsubstituted cinnamoyl moiety. Compounds **12** and **14**, that represent the cyclopropanated congeners of **11** and **13**, retained the NOD2 agonistic activity of the parent compounds, exhibiting 5.2-fold and 5.3-fold activation. Again, the fact that **12** and **14** are mixtures of diastereomers has to be taken into account. Finally, in

agreement with the L-Val series, the 6-phenylindole-incorporating **10** proved to be a weaker NOD2 activator (4.8-fold) than any of the cinnamoyl moiety-featuring analogs.

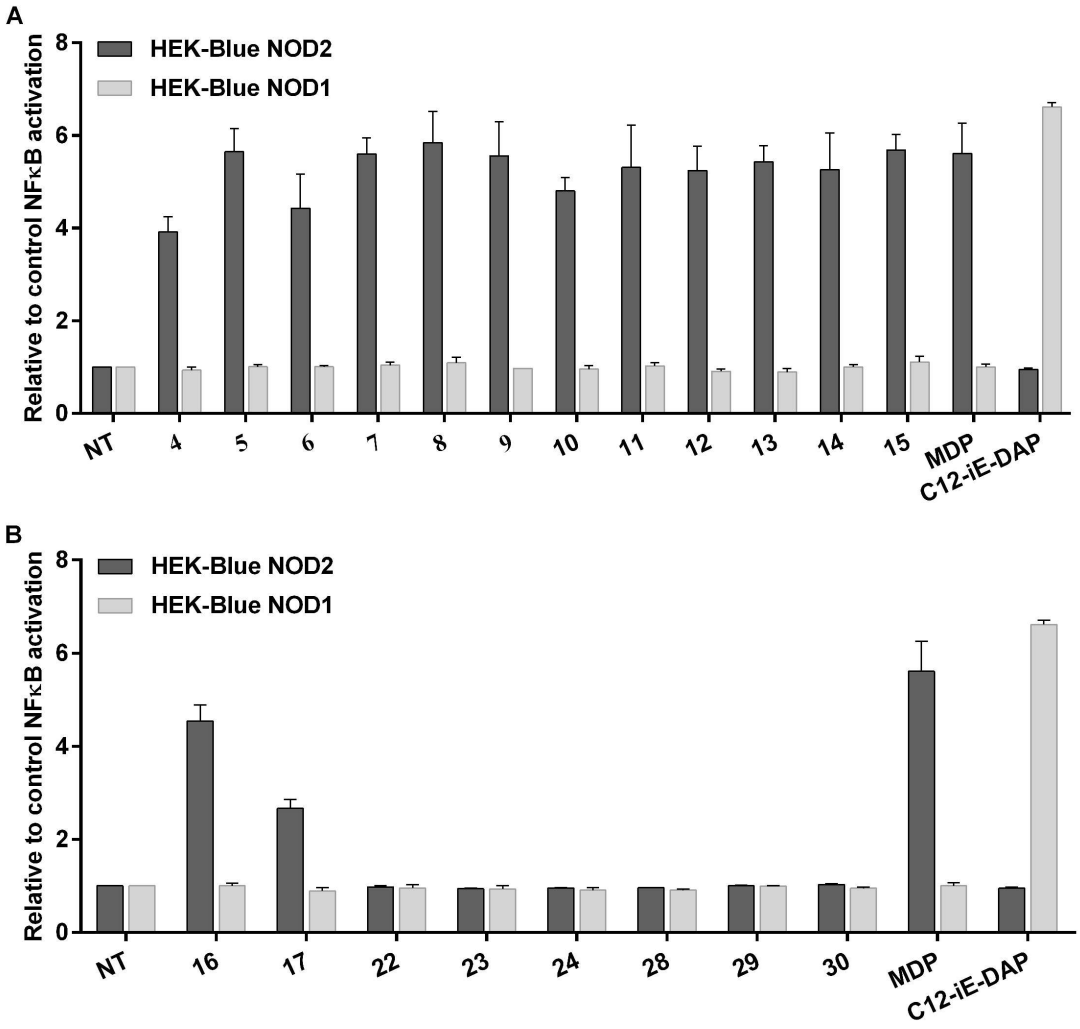

Figure 2. (A) Effects of desmuramylpeptides **4-15** on NF-κB transcriptional activity. **(B)** Effects of desmuramylpeptides **16, 17**, **22-24** and **28-30** on NF-κB transcriptional activity. SEAP activities were measured in both NOD2-specific and NOD1-specific HEK-Blue cells after incubation for 18 h with compounds of interest (2 μM), MDP (2 μM) or C12-iE-DAP (100 nM). The data are shown relative to that of the control (NT). Columns represent the means of duplicates of three independent experiments. Error bars indicate ± S.E.M.

In an effort to improve the SAR of synthesized desmuramylpeptides and to enable comparison with the previously reported compounds, the L-Ala-incorporating congener of **9**, compound **16**, was prepared. Introduction of the L-Ala moiety still allowed for NOD2 activation, although to a lesser extent, as evidenced by the 4.5-fold activation. Previous experiments suggested that the increased NOD2 activation was a result of facilitated entry of desmuramylpeptide esters into the cytosol.[25,34] The influence of modifications of the D-Glu moiety was therefore further addressed by investigating the effect of removing the diethyl ester moieties on NOD2 stimulatory activity (Fig. 2b). Replacement of the diethyl ester groups of **9** by free carboxyl groups gave compound **17** that exhibited significantly diminished (2.7-fold) NOD2 stimulatory capacity. This observation suggests that the presence of ester moieties is a critical factor contributing to the NOD2-agonist activity of the compound.

Replacement of the D-glutamic acid moiety by its custom-made mimetics provided some additional information concerning the ability of these compounds to activate NOD2. It has been speculated that both the carboxylate groups of D-Glu form important interactions with the receptor.[50,51] We thus anticipated that amines carrying only one carboxylate group (incorporated into **22-24**) would act as poor mimetics of glutamic acid. Nevertheless, a slightly better activity was expected of compounds **29** and **30** which carry two COOMe groups at various positions on the aromatic ring. Unfortunately, the mimetic carrying the 4-amino-1,3-dicarboxyl substitution pattern on the phenyl ring could not be prepared due to difficulties in synthesis. Nevertheless, the results of the activation assay substantiate the importance of the D-glutamic acid moiety for NOD2 recognition, since its replacements with rigidified mimetics completely abolished the NOD2 agonistic capacity of the compounds.

This shows that the D-Glu fragment is an important structural characteristic for NOD2 recognition.

The selectivity against NOD1 of all synthesized desmuramylpeptides was also established, employing commercially available HEK-Blue NOD1-dependent NF-κB-inducible SEAP reporter gene assay. These cells were incubated with synthesized desmuramylpeptides (20 μM) for 18 h, followed by the SEAP activity determination in the supernatant. The results which were normalized to that of the control (NT), have shown that none of the desmuramylpeptides nor MDP induced any NF-κB activity relative to the untreated cells (data shown in Fig. 2).

The specificities of all the synthesized compounds on NOD2 were evaluated in parallel, using HEK-Blue NOD2 cells in the presence or absence of GSK-669, a known NOD2 antagonist.[52] HEK-Blue NOD2 cells were pre-incubated with NOD2 antagonist (10 μM) and then stimulated with synthesized desmuramylpeptides or MDP (2 μM) for 18 h, followed by the SEAP activity determination in the supernatant. The control cells were stimulated only with synthesized desmuramylpeptides and MDP (2 μM). The results which were normalized to those of the control cells, indicate that the induced NF-κB activity is indeed a consequence of the NOD2 agonistic activity of desmuramylpeptides and MDP (Fig. S13).

The marginal differences in NOD2 activation observed for most compounds belonging to the L-Val and L-Phe series in the single-point assay, however, make it impossible to draw any clear conclusions regarding SAR. For this reason, the dose-dependent effect of selected compounds was investigated. The selection of desmuramylpeptides was based on the results obtained from the preliminary screening on HEK-Blue NOD2 cells at a concentration of 2

μM. At this concentration several of the synthesized desmuramylpeptides exhibited NOD2 agonistic capacities slightly better than, or comparable to, that of MDP, thus proving that all compounds are full agonists of NOD2. MDP and the selected compounds were then tested over a range of concentrations in order to guarantee that the activation experiments were conducted at an effective concentration and to determine their EC_{50} values.

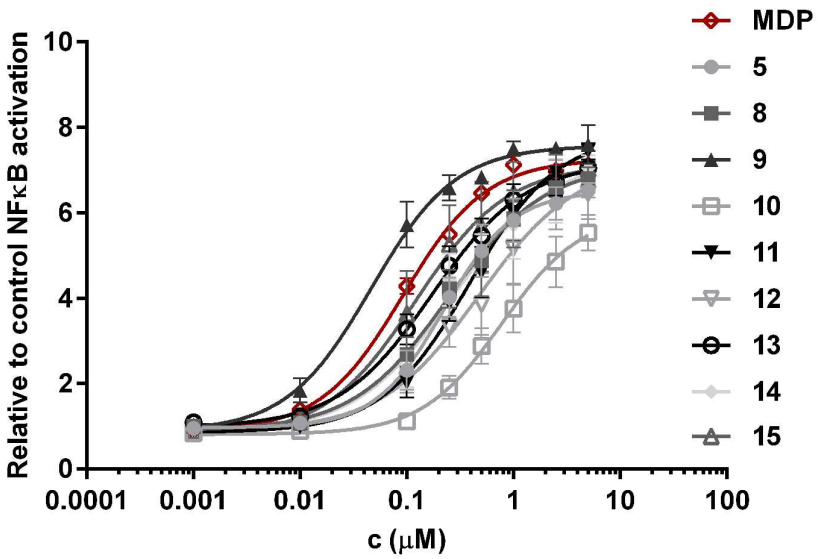

Figure 3. Concentration-dependent activation of NOD2 by selected desmuramylpeptides and by MDP. SEAP activity was measured in NOD2-specific HEK-Blue cells after incubation for 18 h with MDP or with the compound of interest at concentrations ranging from 0.001 μM to 20 μM. Data points represent means of duplicates of three independent experiments; error bars indicate ± S.E.M.

NF-κB transcriptional activity was induced using eleven concentrations of compounds and MDP (ranging from 0.001 μM to 20 μM) allowing for a precise calculation of their EC_{50} values (Table S2). As expected, the results indicate that increasing concentrations of desmuramylpeptides and MDP have an impact on the activation of NOD2. All the tested desmuramylpeptides, as well as MDP (EC_{50} = 92 nM), induced a dose-dependent stimulatory

effect on NOD2 activation (Fig. 3). Several conclusions can be drawn in terms of structural requirements for stimulation of the receptor. Comparison of the EC_{50} values of three compounds harboring only modifications of the second amino acid residue of the tripeptide moiety, compounds **9** (L-Val; EC_{50} = 46 nM), **15** (L-Phe; EC_{50} = 121 nM) and **16** (L-Ala; EC_{50} = 2.79 μM), revealed an important contribution of the bulkiness and lipophilicity of the amino acid side chain to NOD2 agonism. The methyl side chain of L-Ala (**16**) lacks the ability to form strong hydrophobic interactions, in contrast to the isopropyl sidechain (**9**) which resulted in approximately 60-fold loss in activity. The benzyl side chain of **15**, on the other hand, possesses the potential to form hydrophobic interactions but is possibly too large to fit appropriately inside the pocket of the NOD2 receptor. Compound **15** was indeed less active, presumably due to steric hindrance. This finding suggests that a hydrophobic moiety of the appropriate size serves to greatly increase NOD2 stimulation activity. In line with these results, comparison of compound **10** (EC_{50} = 777 nM), carrying the L-Phe moiety, with its L-Ala incorporating counterpart lead **I** (EC_{50} = 2.88 μM) revealed the importance of the amino acid side chain. Compounds **5** (EC_{50} = 223 nM) and **11** (EC_{50} = 388 nM), incorporating the cinnamoyl moiety, exhibited potent NOD2 agonist activity, so we examined the chemical space around the phenyl core. Introduction of two fluorine atoms at positions 3 and 4 resulted in compounds **7** and **13** (EC_{50} = 172 nM). The 3,4-difluorosubstitution slightly increased (2.3-fold) the activity relative to its unsubstituted counterpart. The *trans*-feruloyl acyl moiety featured in **9** and **15** proved to be the most advantageous in both series of compounds (L-Val and L-Phe), thus highlighting this fragment as the most effective mimetic of the carbohydrate portion of the MDP known to date. Replacement of the cinnamoyl moiety (compound **11**; EC_{50} = 388 nM) with its cyclopropane-incorporating bioisostere **12** (EC_{50} = 472 nM) did not affect the NOD2 agonistic activity very much. However, it still has to be borne in mind that **12** is, in fact, a mixture of two diastereomers, indicating that one of them could adopt a

conformation with the most favorable interactions with the receptor. Interestingly, cyclopropanation of the 3,4-difluoro derivative **13** (EC_{50} = 172 nM) diminished the capacity for NOD2 activation, as shown in the case of compound **14** (EC_{50} = 276 nM). However, in analogy to **8** (EC_{50} = 247 nM) from the L-Val series, **14** is a mixture consisting of four diastereomers, of which only one is likely to bind ideally to NOD2. These compounds were isolated as mixtures of four diastereomers, as confirmed by HPLC chromatography. The stereochemistry on the cyclopropane ring presumably has a role in mimicking the preferred spatial orientation of the appended groups. This makes compounds **14** and **8** interesting for further investigations to identify the most potent diastereomer. Evidently, desmuramylpeptides carrying the L-Val moiety are more effective, in terms of NOD2 recognition, than their L-Phe counterparts. Finally, conversion of the diethyl ester functionalities of the most potent compound **9** into free carboxylic acid groups resulted in compound **17** that displays an EC_{50} value of 6.98 μM, indicating a significant 152-fold drop in activity.

*2.3.3 Determination of stability and cell uptake of compound **9** and its hydrolyzed analog **17***

The higher activity of the diester may be related to improved passive uptake of the ligands, which would result in greater availability of the ligand for the NOD2 receptor. The incorporation of ester linkages has been shown to result in increased internalization of the compounds.[53] Our preliminary results suggest that diethyl ester derivatives are merely prodrugs, since introduction of two 1,2,4-oxadiazole moieties as non-hydrolyzable, bioisosteric replacements of the two diethyl ester moieties[54] resulted in complete loss of NOD2 agonist activity.[34] Compounds incorporating ester functionalities are most often cleaved with carboxylic ester hydrolases, particularly carboxylesterases. Most mammalian carboxylesterases belong to the CES1 and CES2 families, which are differentiated on the

basis of substrate specificity and tissue distribution. CES1, which preferentially catalyzes hydrolysis of substrates carrying a small alcohol group and a large acyl moiety, is expressed predominantly in human liver and monocytes/macrophages, including the THP-1 cell line.[55,56] For example, the ethyl ester, once absorbed, is rapidly and predominantly hydrolyzed by the human carboxylesterase 1 (CES1/hCE-1) in the liver.[57,58] In contrast, the CES2 (hCE-2) isozyme is the dominant component in the small intestine, where it catalyzes primarily the hydrolysis of compounds carrying a small acyl group and a large alcohol group.[59] This raises important questions about the fate of compound **9**, namely, which is the precise active moiety that is recognized by the receptor and which are the diethyl esters hydrolyzed under the conditions employed, thus converting **9** into **17**. HEK293 cells are not particularly known to express carboxylesterase enzymes,[60,61] so we speculated that the diester moieties of **9** remain intact, suggesting that the diester is not a prodrug *per se*, but in fact contributes to NOD2 recognition. Use of a highly sensitive LC-MS method enabled us to shed some light on the fates of compounds **9** and **17** under the conditions employed. First, both compounds, at a concentration of 2 μM, remained stable in culture medium for at least 18 hours (Fig. S11). Next, we addressed the stability of compound **9** towards the cell enzymatic system. We collected the extracellular media from an HEK293-NOD2 cell culture treated by incubation with 2 μM concentrations of both compounds for 18 h. Cell lysates obtained from the same experiment were also collected in order to quantify the amount of the tested compound that moved into the cytosol and, also, to examine the extent of compound **9** intracellular ester hydrolysis. First, the extracellular concentrations measured indicate that circa 40% of compound **9** entered the cytosol, while **17** presumably crossed the membrane to a much lesser extent. The lysate concentrations, which were found to be 0.13 (compound **9**) and 0.40 μM (compound **17**), further confirming that both species enter the cytosol (Fig. 4). In light of the strikingly high lysate concentration of compound **17**, it should be noted that the determined

lysate concentrations are not as accurate as the determined extracellular concentrations. Further, compound **9** has proven to be susceptible to hydrolysis by the cells' enzyme machinery, shown by approximately 65% of internalized compound **9** being converted to compound **17** after an 18 h incubation (Fig. 4), thus actually supporting the hypothesis that the diester moieties predominantly allow for successful internalization and most likely contribute to binding to NOD2 only to a minor extent.

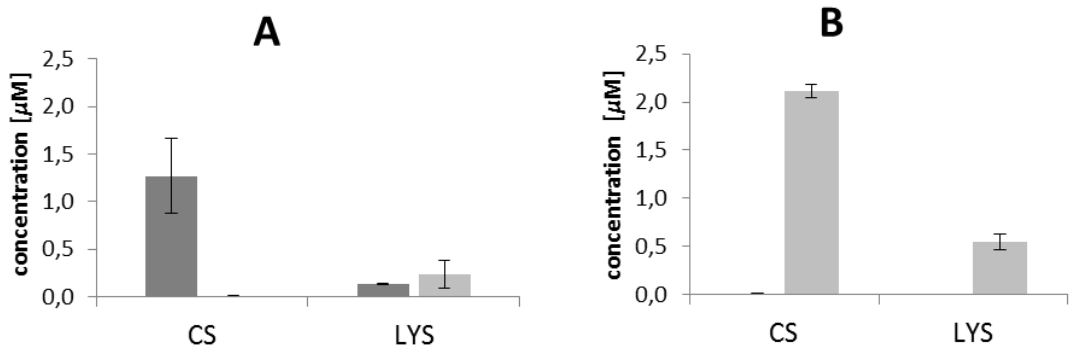

Figure 4. The concentrations of compounds **9** and **17** in cell supernatant (CS) and cell lysate (LYS) determined in the cell uptake and stability experiment performed by 18 h incubations in the presence of 2 μM compound **9** (diagram A) and *2* μM compound **17** (diagram B) in cell incubation media. Dark grey bars represent compound **9** and light grey bars compound **17**. Columns represent means of two independent experiments performed in duplicates. Error bars represent S.E.M.

*2.3.4 Docking studies of compounds **9, 17** and MDP into the crystal structure of NOD2*

During the course of our study, the crystal structure of rabbit NOD2 was determined in the inactive ADP-bound state. A hydrophobic pocket on the concave surface of the LRR domain has been proposed as a potential MDP-binding site.[51] Recent experiments involving docking MDP to a homology model of zebrafish NOD2-LRR have shown that the Mur*N*Ac moiety is responsible for holding the ligand in its correct orientation, suggesting that MDP requires a

hydrophobic pocket for its Mur*N*Ac moiety and a positively charged pocket for its L-Ala-D-*i*Gln part.[62] Further, using surface plasmon resonance methodology, Lauro et al. recently established that the molecular recognition of MDP indeed occurs in the LRR domain and they defined the critical residues responsible for NOD2 recognition. In addition, they showed that both the dipeptide and the carbohydrate moiety contribute to the binding.[50] The putative binding residues for the NOD2-MDP interaction, namely Arg857, Trp911, and Ser913, were highlighted in all models and are thus presumed to be critical for binding. Aromatic residues such as Trp911 are markedly involved in carbohydrate-binding sites, in line with recent findings showing that aromatic rings of the receptor often contribute to carbohydrate recognition in spite of the highly hydrophilic characters of most sugars.[63,64] Compound **9**, incorporating the *trans*-feruloyl mimetic of Mur*N*Ac, displayed the most potent NOD2 agonistic activity, suggesting that the 4-hydroxy-3-methoxycinnamoyl fragment is a pivotal structural feature for NOD2 recognition. However, stability and cell uptake studies suggest that its carboxylic acid derivative **17**, which is the result of hydrolysis of compound **9** after uptake, could be the active compound. Therefore, a proposed model for the orientation of MDP and compounds **9** and **17** in the putative binding pocket was developed using the crystal structure of rabbit NOD2 (PDB entry: 5IRN) and GOLD software. The recognition is predicted to take place in the center of the LRR horseshoe fold. This model shows that Arg857 makes hydrogen bonding interactions with both the carbohydrate portion of MDP and the dipeptide. (Fig. 5a), as observed previously.[50] However, there are certain differences in the predicted MDP binding modes to NOD2, which can be attributed to flexibility of the proposed binding pocket. This was partially addressed by making selected sidechains flexible in the study of Lauro et al, while in our docking protocol, the protein was kept rigid. Nevertheless, the MDP sugar moiety was found to occupy the same hydrophobic pocket and the dipeptide was predicted to be in contact with the Arg857 side chain in both studies. The stability of the

NOD2-MDP complex was evaluated through molecular dynamics simulation in which the orientation of MDP slightly changed, but it still remained in contact with relevant residues (i.e. Arg857 and Trp911, Fig. S1).

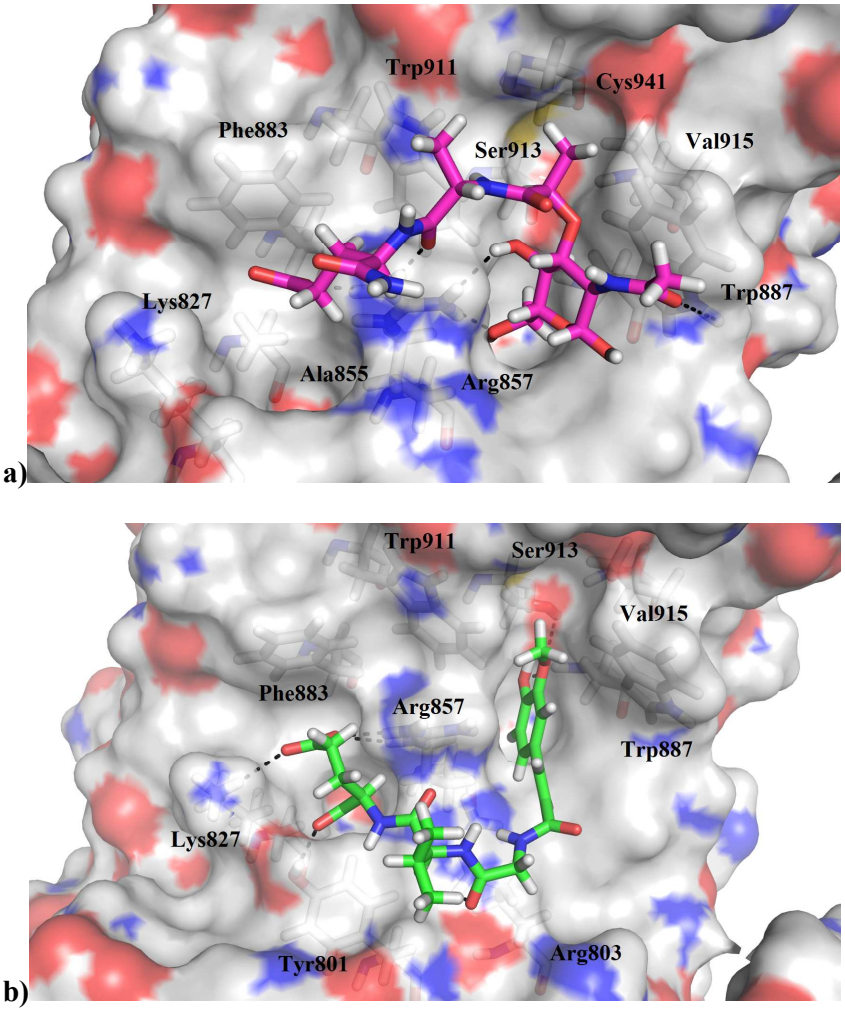

Figure 7. Predicted binding modes of **a)** MDP (magenta sticks) and **b) 17** (green sticks) in the putative binding pocket on the concave surface of the LRR domain of NOD2 (PDB entry: 5IRN). The protein is shown in surface presentation and, for clarity, only amino acid side chains interacting with the ligands are shown as grey sticks. Hydrogen bonds are shown as black dashed lines.

Docking of compound **17** suggests its similar orientation to that of MDP (Fig. 5b) in the putative binding pocket on the concave surface of the LRR domain of NOD2. The 4-hydroxy-3-methoxycinnamoyl moiety of **17** was suggested to mimic the sugar moiety of MDP, since it binds to the same hydrophobic pocket, where it forms π-π stacking with Trp911 side chain and cation-π interaction with Arg857, while its methoxy group interacts with Ser913 side chain. Additional interaction is predicted between the hydroxy group of the 4-hydroxy-3-methoxycinnamoyl moiety and backbone NH of Trp887. Tripeptide moiety of **17** forms several hydrogen bonds with NOD2 residues. In detail, Gly carbonyl oxygen of **17** is hydrogen bonded to Arg803 side chain, while α-carboxylate of the D-Glu of **17** interacts with the Tyr801 side chain and γ-carboxylate with the Lys827 and Arg857 side chains. The stability of the proposed binding mode of **17** was tested with molecular dynamics simulation, in which only slight reorientation of the tripeptide portion of **17** was observed (Fig. S2).

Compound **9** was predicted to bind in two different orientations to NOD2 – the first similar to that of compound **17** and the second in a different orientation in relation to MDP (Fig. S3). However, when NOD2 in complex with **9** was studied by molecular dynamics simulations neither of these poses proved stable (Figs. S4 and S5), which is in agreement with the docking studies that predicted more extensive hydrogen bonding network of the carboxylate **17** than its ester derivative **9** (Figs. 5b and S3).

Taken together, our docking model thus suggests good complementarity of MDP and compound **17** and the binding pocket in the NOD2 LRR domain. Additional structural insights have thus been provided into the pharmacophores required for NOD2 activation.

*2.3.5 Immunostimulatory properties of desmuramylpeptide **9** and MDP on PBMCs*

The immunostimulatory activity of the best compound **9** was investigated on human peripheral blood mononuclear cells (PBMC) using the Human Th1/Th2/Th17 cytokine kit, in order to extend the analysis beyond reporter gene assays (Fig. 6). Desmuramylpeptide **9** and MDP were evaluated for their ability to modulate pro- and anti-inflammatory cytokine production in PBMCs, alone or in combination with LPS. PBMCs constitute a physiologically relevant model system for investigating the immunomodulatory properties of a broad range of innate immune stimulants.[65] The immunostimulatory capacity of NOD2 agonists is grounded mainly on stimulation of monocytes/macrophages. Similarly, LPS acts as an effective stimulus for the induction of Th1-type cytokines and mainly stimulates monocytes.[66] Unstimulated PBMCs produce few or no cytokines spontaneously and, as expected, stimulation of PBMCs with MDP and **9** alone (2 μM concentration) produced modest amounts of cytokines. Nevertheless, the release of TNF-α, IL-6 and IL-10 was increased significantly by both compounds (compared to untreated cells).

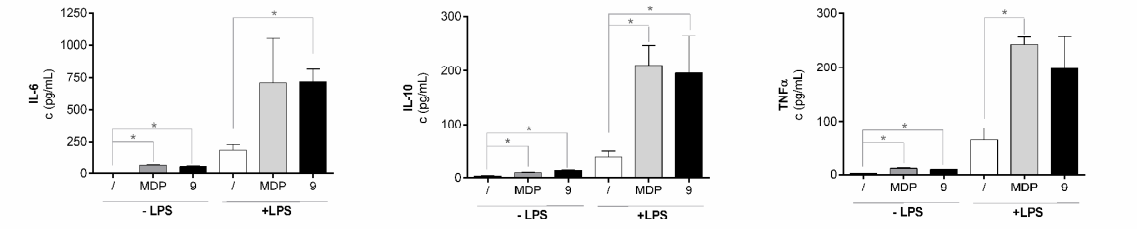

Figure 6. Effect of MDP and compound **9** on cytokine release in PBMCs. Cells were treated with 2 μM MDP or **9** in the presence or absence of 10 ng/mL LPS. Cytokine release was determined after 18 h. Columns represent means of duplicates ± S.E.M. of two independent experiments (data are representative of two independent donors); * $p < 0.05$ vs untreated (NT) or LPS-treated cells.

On the other hand, stimulation with LPS brought about a considerable increase in cytokine release. This effect was evidently potentiated by the presence of MDP or compound **9** for all cytokines tested. The LPS-evoked release of the anti-inflammatory cytokine IL-10 was significantly amplified 5-fold by MDP or compound **9**. This effect was also observed in the case of the release of proinflammatory cytokines. Namely, the TNF-α release was increased 3-fold by compound **9** and 3.6-fold by MDP, while IL-6 release was increased 4-fold by both compounds.

The results are in agreement with those in studies that identified a powerful amplification effect of MDP on TLR4-induced cytokine production from isolated PBMCs while, on its own, inducing only low levels cytokines.[14,67,68] The capacity of MDP to synergize with LPS and other TLR ligands, resulting in an amplified proinflammatory cytokine response, is well documented.[69] Such a synergy can be of great physiological importance since, during bacterial infection, MDP and LPS are likely to be present in the same tissues.

*2.3.6 Adjuvant properties of liposome-encapsulated **9** and MDP in OVA-induced antibody response*

An evident correlation between NOD2-stimulating capacities as well as adjuvant and antimicrobial properties of MDP derivatives has been shown,[42] so desmuramylpeptide **9** was investigated further to evaluate its usefulness as an adjuvant. First, we established that **9** was devoid of any pyrogenic activity due to potential endotoxin contamination using a standard bacterial endotoxin test (data not shown).

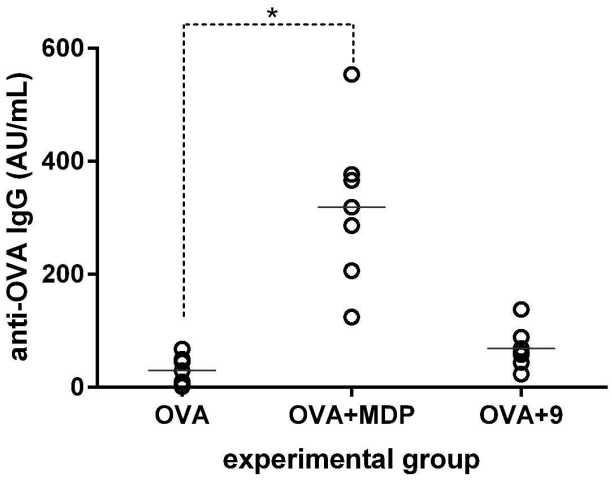

Figure 7. Comparison of the adjuvant effects of MDP and **9** on the production of total anti-OVA IgGs in the sera of three experimental groups of NIH/OlaHsd female mice (n=6) after the second booster. 1. OVA in liposomes (50 μg of OVA in sterile PBS), 2. OVA+MDP in liposomes (50 μg of OVA with 200 μg/mouse of MDP); 3. OVA+**9** in liposomes (50 μg of OVA with 200 μg/mouse of **9)**. ○ Denotes each mouse separately, —— denotes group mean value; * p<0.05 (Kruskal–Wallis ANOVA, followed by multiple Mann–Whitney U-nonparametric tests) in comparison to the group not treated by adjuvant or in comparison with the group connected with dashed lines.

NOD2 induces a predominant Th2 polarized response, while a combination of PRR ligands such as NLR/TLR evokes a Th1 and Th17 response. Also, Tukhvatulin et al showed that, by employing a multi-PRR activation approach as part of a standard alum-based vaccine formulation, activation of both cellular and humoral immunity was significantly increased. In fact, it proved to be superior to alum or a combination of alum and an individual PRR ligand.[70] The adjuvanticity of MDP was also shown to depend on the mode of administration; thus, MDP evoked a potent response when delivered with lipophilic carrier systems, such as liposomes.[71] Liposomes have long been used as carriers of antigens and adjuvants to enhance

the immune response.[72] The aim of this experiment was to evaluate liposome-encapsulated MDP and **9** for their immunoadjuvant activity in a well defined mouse model. Specifically, their effect on the induction of a humoral immune response specific for protein antigen ovalbumin (OVA) as well as their capacity to skew the immune response towards Th1/Th2 were investigated. The group treated with OVA alone acted as a negative control. Both MDP and **9** increased anti-OVA IgG levels in sera relative to those in the control (Fig. 7).

Table 1. The ratio of anti-OVA IgG1 and anti-OVA IgG2a levels following a second booster

Experimental group	$\log_{10}$ (anti-OVA IgG1/anti-OVA IgG2a)
1. OVA in liposomes	1.69 ± 0.28
2. (OVA + MDP) in liposomes	2.37 ± 0.39*
3. (OVA + **9**) in liposomes	2.62 ±0.55*

The IgG1/IgG2a ratio was calculated after the second booster for each mouse serum. The results for each experimental group (n=6; females) are reported as the means± SD; *$p \leq 0.01$ in comparison to the first group.

It is well known that vaccine adjuvants can modulate the Th1/Th2-bias of an induced immune response. In our study, the nature of the immune response produced was estimated indirectly by quantification of antigen-specific IgG1 (Th2-associated isotype) and IgG2a (Th1-associated isotype) and calculation of their ratio (Table 1). The immune response specific for OVA was Th2-biased with an IgG1/IgG2a ratio of 44.3 (log IgG1/IgG2a = 1.69) as demonstrated by Habjanec,[73,74] while the adjuvanticity of MDP depends upon the administration context. Administration in saline increased the humoral immunity, while its incorporation into liposomes resulted in cell-mediated immunity.[75] In addition, hydrophilic MDP derivatives are known to induce a Th2-type response as opposed to lipophilic derivatives which augment the Th-1 type immune response. Of note, it was shown that co-

administration of MDP and alum skews the immune response towards the Th1 type. IgG1 was the predominant IgG subclass for all groups while only MDP, albeit weakly, induced an IgG2 response, resulting in an IgG1/IgG2a ratio of 133 (log IgG1/IgG2a = 2.37). In contrast, **9** displayed an IgG1/IgG2a ratio of 258 (log IgG1/IgG2a = 2.62) indicating a slight shift of the immune reaction towards the Th2 type of response. The result of this preliminary experiment sheds some light on the immunoadjuvant activity of both MDP and **9**. Compound **9** could function as an adjuvant, as evidenced by the OVA-specific serum IgG1 antibodies detected after a prime-boost immunization regimen with OVA+**9**.

CONCLUSIONS

A series of fourth-generation desmuramylpeptides have been designed and prepared. Diverse variations were incorporated into the parent molecules providing further insights into the structure-activity relationship. The obtained results significantly increase our understanding of the structural requirements of desmuramylpeptides for NOD2-activation. In particular, compound **9** was identified as the, so far, most potent NOD2 agonist of the desmuramylpeptide structural class. Compound **9** also possesses the ability to augment LPS-induced pro-inflammatory cytokine release from PBMCs as well as to increase OVA-specific IgG titers in a mouse model of adjuvancy. Together, our results indicate that **9** can induce both innate and adaptive immune responses and thus demonstrate the potential utility of NOD2 agonists as adjuvants for vaccines.

4. EXPERIMENTAL SECTION

4.1 General

Chemicals were obtained from Acros, Aldrich Chemical Co., Molekula, Enamine and Fluka, and used without further purification. MDP and LPS (from *E.coli* O111:B4) were obtained from Invivogen, Inc., (San Diego, CA). NOD2 antagonist was synthesized as described.[52] Analytical TLC was performed on Merck 60 F254 silica gel plates (0.25 mm), using visualization with ultraviolet light and ninhydrin. Column chromatography was carried out on silica gel 60 (particle size 240-400 mesh). Melting points were determined on a Reichert hot stage microscope and are uncorrected. ^{1}H- and ^{13}C-NMR spectra were recorded at 400 MHz and 100 MHz, respectively, on a Bruker AVANCE III spectrometer in $CDCl_3$, acetone-d_6 or MeOD solution with tetramethylsilane (TMS) as the internal standard. Spectra were assigned using gradient HSQC and HMBC. IR spectra were recorded on a Perkin-Elmer 1600 FT-IR spectrometer. Mass spectra were obtained using a VG-Analytical Autospec Q mass spectrometer. HPLC analyses for determination of purity were performed on an Agilent Technologies HP 1100 instrument with G1365B UV-VIS detector (254 nm), using a Luna C18 column (4.6 × 150 mm) at a flow rate of 1 mL/min. The eluent was a mixture of 0.1% TFA in water (A) and acetonitrile (B), with a gradient of 30% B to 80% B from 0-30 minutes and 80% B to 90% B from 30-33 minutes. The purity of all biologically tested compounds is ≥95%.

4.2 General procedures

4.2.1 TFA-mediated acidolysis

Boc-protected compound (5 mmol) was added to an ice-chilled stirred mixture of trifluoroacetic acid and dichloromethane (5/1, 10 mL), and the mixture allowed to warm to room temperature. After 3 hours the reaction was completed. The solvent was evaporated *in*

vacuo. The residue was washed three times with diethyl ether and used immediately for the next step.

4.2.2 DCC-mediated coupling

To a stirred solution of the corresponding carboxylic acid derivative (5.5 mmol) and amine (5 mmol) in dry ethyl acetate, diisopropylethylamine (DIPEA) (12.5 mmol) was added at 0 °C. After stirring for 15 minutes, DCC (5.5 mmol) and HOBt (5.5 mmol) and a catalytic amount of 4-dimethylaminopyridine (DMAP) were added, and the mixture allowed to warm to room temperature with stirring, the latter being continued overnight. The reaction mixture was filtered and the filtrate diluted with ethyl acetate (50 mL) and washed with twice with a solution of 1M HCl (2 × 20 mL), water (20 mL), saturated $NaHCO_3$ solution (2 × 20 mL), water (20 mL), then dried over anhydrous Na_2SO_4. The solvent was evaporated *in vacuo*. If necessary, the residues were additionally purified using column chromatography to afford sufficiently pure products.

4.2.3 EDC-mediated coupling

To a stirred solution of the corresponding carboxylic acid derivative (0.33 mmol) and amine (0.3 mmol) in dry dichloromethane, DIPEA (0.75 mmol) was added at 0 °C. After stirring for 15 minutes EDC (0.33 mmol) and HOBt (0.33 mmol) and a catalytic amount of DMAP were added, and the mixture allowed to warm to room temperature. Stirring was continued overnight. On completion, the reaction mixture was diluted with dichloromethane (30 mL) and then washed with 1M HCl (2 × 10 mL), water (20 mL), saturated $NaHCO_3$ solution (2 × 10 mL), water (20 mL), then dried over anhydrous Na_2SO_4. The solvent was evaporated *in vacuo*. If necessary, the products were further purified using column chromatography to afford sufficiently pure products.

4.2.4 Alkaline hydrolysis

To a solution of ethyl ester (2 mmol) in ethanol was added 1M KOH (4 mL) and the mixture stirred for 24 hours at room temperature. Upon completion of the reaction, as monitored by TLC, the ethanol was evaporated and the remaining water phase acidified with 1M HCl to pH ~ 3. The obtained precipitate was filtered off and dried at 75 °C in an oven to afford compounds.

4.3 Characterization of compounds

4.3.1 Diethyl (6-phenyl-1H-indole-2-carbonyl)glycyl-L-valyl-D-glutamate **(4).** Synthesized according to the *General procedure for EDC-mediated coupling*. Yellow-white amorphous solid, yield: 66 mg (38%); m.p. 150-153 °C. ^{1}H-NMR ($CDCl_3$, 400 MHz): δ = 1.17 (d, 3H, *J* = 6.8 Hz, C$\underline{H}_3$-Val), 1.20 (d, 3H, *J* = 6.8 Hz, C$\underline{H}_3$-Val), 1.32–1.40 (m, 6H, 2 x $CH_2C\underline{H}_3$), 2.31–2.38 (m, 1H, C$\underline{H}_{2A}$-β-Glu), 2.43–2.51 (m, 2H, C$\underline{H}_{2B}$-β-Glu and C$\underline{H}(CH_3)_2$), 2.58–2.67 (m, 2H, C$\underline{H}_2$-γ-Glu), 4.19–4.37 (m, 4H, 2 × C$\underline{H}_2CH_3$), 4.47–4.52 (m, 1H, NHC$\underline{H}_{2A}$), 4.76–4.81 (m, 1H, NHC$\underline{H}_{2B}$), 4.85–4.93 (m, 2H, α-C$\underline{H}$-Val and α-C$\underline{H}$-Glu), 7.26 (s, 1H, $\underline{H}$-Ar), 7.50–7.61 (m, 4H, 4 × $\underline{H}$-Ar), 7.81–7.85 (m, 4H, 4 × $\underline{H}$-Ar), 8.02 (d, 1H, *J* = 7.2 Hz, NH), 8.23 (s, 1H, N$\underline{H}CH_2$), 8.51 (d, 1H, *J* = 9.2 Hz, NH), 10.76 (s, 1H, indole-N$\underline{H}$) ppm. ^{13}C-NMR ($CDCl_3$, 100 MHz): δ = 14.08, 17.97, 19.35, 26.95, 30.48, 31.39, 43.79, 52.29, 58.50, 60.93, 61.79, 103.45, 110.63, 120.26, 122.17, 126.86, 126.92, 127.28, 128.73, 130.70, 137.48, 141.95, 162.39, 169.82, 171.67, 171.97, 173.03 ppm. MS (ESI): m/z (%) = 577.3 $(M-H)^-$. IR (ATR): ν = 3262, 2961, 1714, 1675, 1633, 1547, 1373, 1332, 1285, 1204, 1113, 1019, 825, 741, 693 cm^{-1}. HPLC (254 nm): 100.0%, t_r = 19.64 min. HRMS Calcd for $C_{31}H_{37}N_4O_7$ m/z: 577.2662 $(M-H)^-$, found 577.2664. $[\alpha]_D^{20}$ = -14.8° (*c* 0.22, CH_2Cl_2).

4.3.2 Diethyl cinnamoylglycyl-L-valyl-D-glutamate **(5).** Synthesized according to the *General procedure for EDC-mediated coupling*. White amorphous solid, yield: 88 mg (60%); m.p.

157-160 °C. ^{1}H-NMR ($CDCl_3$, 400 MHz): δ = 0.94–0.99 (m, 6H, 2 × C$\underline{H}_3$-Val), 1.18–1.24 (m, 6H, 2 × $CH_2C\underline{H}_3$), 1.99–2.08 (m, 1H, C$\underline{H}_{2A}$-β-Glu), 2.14–2.23 (m, 2H, C$\underline{H}_{2B}$-β-Glu in C$\underline{H}(CH_3)_2$), 2.33–2.47 (m, 2H, C$\underline{H}_2$-γ-Glu), 4.04–4.32 (m, 6H, NHC$\underline{H}_2$ and 2 × C$\underline{H}_2CH_3$), 4.53–4.62 (m, 2H, α-C$\underline{H}$-Val and α-C$\underline{H}$-Glu), 6.63 (d, 1H, *J* = 15.6 Hz, CH=C$\underline{H}$), 7.32–7.34 (m, 4H, 3 × $\underline{H}$-Ar in NHCH_2), 7.45 (d, 1H, *J* = 8.8 Hz, N$\underline{H}$), 7.49–7.51 (m, 2H, 2 × $\underline{H}$-Ar), 7.62–7.66 (m, 2H, C$\underline{H}$=CH and N$\underline{H}$) ppm. ^{13}C-NMR ($CDCl_3$, 100 MHz): δ = 14.11, 14.14, 17.95, 19.33, 26.90, 30.40, 31.23, 43.63, 51.86, 58.50, 60.74, 61.59, 120.22, 127.92, 128.81, 129.76, 134.82, 141.55, 166.61, 169.44, 171.32, 171.59, 172.79 ppm. MS (ESI): m/z (%) = 488.2 $(M-H)^-$. IR (ATR): ν = 3266, 3069, 2965, 1730, 1689, 1640, 1612, 1528, 1448, 1392, 1213, 1162, 1110, 1022, 977, 861, 766, 733, 694, 664 cm^{-1}. HPLC (254 nm): 100.0%, t_r = 12.68 min. HRMS Calcd for $C_{25}H_{34}N_3O_7$ m/z: 488.2397 $(M-H)^-$, found 488.2393. $[\alpha]_D^{20}$ = +17.7° (*c* 0.12, CH_2Cl_2).

4.3.3 Diethyl (trans-2-phenylcyclopropane-1-carbonyl)glycyl-L-valyl-D-glutamate **(6).** Synthesized according to the *General procedure for EDC-mediated coupling*. White amorphous solid, yield: 101 mg (67%); m.p. 159-162 °C. ^{1}H-NMR ($CDCl_3$, 400 MHz): δ = 0.90–0.94 (m, 6H, 2 × C$\underline{H}_3$-Val), 1.19–1.24 (m, 7H, 2 × $CH_2C\underline{H}_3$ and PhCHC$\underline{H}_{2A}$CH), 1.54–1.59 (m, 1H, PhCHC$\underline{H}_{2B}$CH), 1.84–1.89 (m, 1H, PhCHCH_2C$\underline{H}$), 1.93–2.02 (m, 1H, C$\underline{H}_{2A}$-β-Glu), 2.08–2.18 (m, 2H, C$\underline{H}_{2B}$-β-Glu and C$\underline{H}(CH_3)_2$), 2.31–2.36 (m, 2H, C$\underline{H}_2$-γ-Glu), 2.44–2.48 (m, 1H, PhC$\underline{H}$CH_2CH), 4.00–4.23 (m, 6H, 2 x C$\underline{H}_2CH_3$ and NHC$\underline{H}_2$), 4.47–4.54 (m, 2H, α-C$\underline{H}$-Val and α-C$\underline{H}$-Glu), 7.06–7.08 (m, 2H, 2 × $\underline{H}$-Ar), 7.13–7.18 (m, 1H, $\underline{H}$-Ar), 7.22–7.33 (m, 4H, 2 × $\underline{H}$-Ar and NHCH_2 and NH), 7.53–7.58 (m, 1H, NH) ppm. ^{13}C-NMR ($CDCl_3$, 100 MHz): δ = 14.11, 14.16, 16.06, 17.88, 17.94, 19.22, 25.30, 25.90, 25.97, 26.94, 30.39, 31.22, 31.29, 43.62, 43.72, 51.76, 51.80, 58.26, 60.76, 61.57, 126.11, 126.14, 126.25, 126.28, 128.41, 128.43, 140.68, 169.33, 171.19, 171.58, 171.61, 172.81, 172.84 ppm. MS (ESI): m/z

(%) = 502.3 $(M-H)^-$. IR (ATR): ν = 3271, 2965, 1734, 1624, 1530, 1446, 1374, 1262, 1207, 1176, 1094, 1023, 935, 857, 757, 696 cm^{-1}. HPLC (254 nm): 58.0% (t_r = 13.95 min), 42.0% (t_r = 14.21 min); total: 100% (mixture of 2 diastereomers). HRMS Calcd for $C_{26}H_{36}N_3O_7$ m/z: 502.2553 $(M-H)^-$, found 502.2555. $[\alpha]_D^{20}$ = -1.8° (*c* 0.25, CH_2Cl_2).

4.3.4 Diethyl ((E)-3-(3,4-difluorophenyl)acryloyl)glycyl-L-valyl-D-glutamate **(7).** Synthesized according to the *General procedure for EDC-mediated coupling*. White amorphous solid, yield: 96 mg (61%); m.p. 163-166 °C. ^{1}H-NMR ($CDCl_3$, 400 MHz): δ = 0.93–0.98 (m, 6H, 2 × C$\underline{H}_3$-Val), 1.18–1.27 (m, 6H, 2 × $CH_2C\underline{H}_3$), 1.99–2.08 (m, 1H, C$\underline{H}_{2A}$-β-Glu), 2.12–2.23 (m, 2H, C$\underline{H}_{2B}$-β-Glu and C$\underline{H}(CH_3)_2$), 2.33–2.47 (m, 2H, C$\underline{H}_2$-γ-Glu), 4.05–4.30 (m, 6H, 2 × $C\underline{H}_2CH_3$ and NH-C$\underline{H}_2$), 4.48–4.61 (m, 2H, α-C$\underline{H}$-Glu and α-C$\underline{H}$-Val), 6.55 (d, 1H, *J* = 15.6 Hz, C$\underline{H}$=CH), 7.19–7.23 (m, 1H, $\underline{H}$-Ar), 7.10–7.16 (m, 1H, $\underline{H}$-Ar), 7.22–7.25 (m, 2H, $\underline{H}$-Ar and N$\underline{H}$), 7.46 (d, 1H, *J* = 8.0 Hz, N$\underline{H}$), 7.54 (d, 1H, *J* = 15.6 Hz, CH=C$\underline{H}$), 7.63 (d, 1H, *J* = 8.0 Hz, N$\underline{H}$) ppm. ^{13}C-NMR ($CDCl_3$, 100 MHz): δ = 14.10, 14.11, 17.96, 19.29, 26.86, 30.38, 31.18, 51.89, 58.55, 60.81, 61.65, 116.13 (d, *J* = 20.1 Hz), 117.70 (d, *J* = 17.4 Hz), 121.20, 124.67, 132.08 (d, *J* = 8.1 Hz), 139.35, 139.38, 166.03, 169.32, 171.30, 171.66, 172.83 ppm. MS (ESI): m/z (%) = 526.2 $(M+H)^+$. IR (ATR): ν = 3287, 2930, 1735, 1636, 1515, 1376, 1275, 1202, 1113, 1023, 970, 855, 818, 774, 669 cm^{-1}. HPLC (254 nm): 98.0%, t_r = 13.22 min. HRMS Calcd for $C_{25}H_{34}F_2N_3O_7$ m/z: 526.2365 $(M+H)^+$, found 526.2360. $[\alpha]_D^{20}$ = +2.8° (*c* 0.15, CH_2Cl_2).

4.3.5 Diethyl (2-(3,4-difluorophenyl)cyclopropane-1-carbonyl)glycyl-L-valyl-D-glutamate **(8).** Synthesized according to the *General procedure for EDC-mediated coupling*. White amorphous solid, yield: 105 mg (61%); m.p. 164-167 °C. ^{1}H-NMR ($CDCl_3$, 400 MHz): δ = 0.91–0.94 (m, 6H, 2 × C$\underline{H}_3$-Val), 1.20–1.25 (m, 7H, 2 × $CH_2C\underline{H}_3$ and PhCHC$\underline{H}_{2A}$CH), 1.53–

1.58 (m, 1H, PhCHC$\underline{H}_{2B}$CH), 1.82–1.84 (m, 1H, PhCHCH$_2$C$\underline{H}$), 1.95–2.00 (m, 1H, C$\underline{H}_{2A}$-β-Glu), 2.11–2.17 (m, 2H, C$\underline{H}_{2B}$-β-Glu and C$\underline{H}$(CH$_3$)$_2$), 2.26–2.49 (m, 3H, C$\underline{H}_2$-γ-Glu and PhC$\underline{H}$CH$_2$CH), 4.03–4.21 (m, 6H, NHC$\underline{H}_2$ and 2 × C$\underline{H}_2$CH$_3$), 4.50–4.51 (m, 2H, α-C$\underline{H}$-Val and α-C$\underline{H}$-Glu), 6.82–6.91 (m, 2H, 2 x $\underline{H}$-Ar), 7.00–7.07 (m, 1H, $\underline{H}$-Ar), 7.26–7.29 (m, 2H, 2 × NH), 7.53–7.54 (m, 1H, NH) ppm. ^{13}C-NMR (CDCl$_3$, 100 MHz): δ = 14.07, 14.14, 16.02, 17.88, 17.91, 19.21, 24.35, 25.90, 26.90, 26.94, 30.35, 31.28, 43.61, 51.80, 51.83, 58.28, 60.82, 61.63, 114.93 (d, *J* = 4.4 Hz), 115.10 (d, *J* = 4.3 Hz), 117.20 (d, *J* = 3.3 Hz), 122.38, 137.72-137.82 (m), 148.37 (dd, *J* = 129.5 Hz, *J* = 14.5 Hz), 150.76 (dd, *J* = 141.1 Hz, *J* = 9.8 Hz), 169.20, 171.12, 171.58, 172.28, 172.81 ppm. MS (ESI): m/z (%) = 538.2 (M-H)$^-$. IR (ATR): ν = 3280, 2923, 1732, 1631, 1546, 1522, 1454, 1381, 1268, 1219, 1165, 1116, 1064, 1023, 910, 862, 812, 771, 715, 668, 613 cm^{-1}. HPLC (254 nm): 18,06 % (t_R = 14,46 min), 56,27 % (t_R = 15,80 min), 23,25 % (t_R = 16,46 min); total: 97,58 % (mixture of 4 diastereomers). HRMS Calcd for $C_{26}H_{34}F_2N_3O_7$ m/z: 538.2365 (M-H)$^-$, found 538.2353. $[\alpha]_D^{20}$ = +39.3° (*c* 0.15, CH_2Cl_2).

4.3.6 Diethyl ((E)-3-(4-hydroxy-3-methoxyphenyl)acryloyl)glycyl-L-valyl-D-glutamate **(9).** Synthesized according to the *General procedure for EDC-mediated coupling*. Yellow-white amorphous solid, yield: 58 mg (36%); m.p. 117-120 °C. ^{1}H-NMR (CDCl$_3$, 400 MHz): δ = 0.93 (d, 3H, *J* = 6.8 Hz, C$\underline{H}_3$-Val), 0.97 (d, 3H, *J* = 6.8 Hz, C$\underline{H}_3$-Val), 1.21–1.29 (m, 6H, 2 x CH$_2$C$\underline{H}_3$), 1.99–2.08 (m, 1H, C$\underline{H}_{2A}$-β-Glu), 2.15–2.30 (m, 2H, C$\underline{H}_{2B}$-β-Glu and C$\underline{H}$(CH$_3$)$_2$), 2.32–2.47 (m, 2H, C$\underline{H}_2$-γ-Glu), 3.92 (s, 3H, OCH$_3$), 4.05–4.22 (m, 6H, 2 × C$\underline{H}_2$CH$_3$ and NHC$\underline{H}_2$), 4.38–4.44 (m, 1H, α-C$\underline{H}$), 4.51–4.56 (m, 1H, α-C$\underline{H}$), 5.87 (br s, 1H, OH), 6.34 (d, 1H, *J* = 15.6 Hz, CH=C$\underline{H}$), 6.59 (t, 1H, *J* = 5.2 Hz, N$\underline{H}$CH$_2$), 6.81 (d, 1H, *J* = 8.4 Hz, N$\underline{H}$), 6.90 (d, 1H, *J* = 8.0 Hz, $\underline{H}$-Ar), 7.02 (d, 1H, *J* = 1.2 Hz, $\underline{H}$-Ar), 7.05–7.09 (m, 2H, $\underline{H}$-Ar and N$\underline{H}$), 7.57 (d, 1H, *J* = 15.6 Hz, C$\underline{H}$=CH) ppm. ^{13}C-NMR (CDCl$_3$, 100 MHz): δ = 14.09,

14.14, 17.87, 19.34, 26.81, 30.42, 30.92, 43.61, 51.90, 55.93, 58.58, 60.76, 61.62, 110.09, 114.82, 117.54, 122.14, 127.23, 141.68, 146.83, 147.58, 167.04, 169.76, 171.45, 171.73, 172.84 ppm. MS (ESI): m/z (%) = 534.2 $(M-H)^-$. IR (ATR): ν = 3287, 2963, 1725, 1635, 1513, 1452, 1374, 1265, 1192, 1122, 1025, 976, 844, 814, 680 cm^{-1}. HPLC (254 nm): 96.3%, t_r = 7.45 min. HRMS Calcd for $C_{26}H_{36}N_3O_9$ m/z: 534.2452 $(M-H)^-$, found 534.2458. $[\alpha]_D^{20}$ = +15.4° (*c* 0.22, CH_2Cl_2).

4.3.7 Diethyl (6-phenyl-1H-indole-2-carbonyl)glycyl-L-phenylalanyl-D-glutamate **(10).** Synthesized according to the *General procedure for EDC-mediated coupling*. Yellow amorphous solid, yield: 83 mg (44%); m.p. 63-67 °C. ^{1}H-NMR ($CDCl_3$, 400 MHz): δ = 1.16–1.25 (m, 6H, 2 x $CH_2C\underline{H}_3$), 1.90–2.01 (m, 1H, $C\underline{H}_{2A}$-β-Glu), 2.04–2.20 (m, 2H, $C\underline{H}_{2B}$-β-Glu and $C\underline{H}_2$-γ-Glu), 3.14 (d, 1H, *J* = 7.6 Hz, $C\underline{H}_2$-Phe), 3.99–4.23 (m, 5H, 2 × $C\underline{H}_2CH_3$ and $NHC\underline{H}_{2A}$), 4.41–4.50 (m, 1H, $NHC\underline{H}_{2B}$), 4.58–4.63 (m, 1H, α-C<u>H</u>), 5.04 (q, 1H, *J* = 7.6 Hz, α-C<u>H</u>), 7.04 (s, 1H, <u>H</u>-Ar), 7.07–7.10 (m, 1H, <u>H</u>-Ar), 7.10–7.22 (m, 4H, 4 × <u>H</u>-Ar), 7.31–7.45 (m, 4H, 4 × <u>H</u>-Ar), 7.49 (d, 1H, *J* = 7.6 Hz, NH), 7.65–7.69 (m, 3H, 3 × <u>H</u>-Ar), 7.74 (t, 1H, *J* = 4.8 Hz, $N\underline{H}CH_2$), 8.29 (d, 1H, *J* = 8.4 Hz, NH), 10.57 (s, 1H, indole-N<u>H</u>) ppm. ^{13}C-NMR ($CDCl_3$, 100 MHz): δ = 14.05, 14.14, 26.89, 28.32, 30.06, 39.02, 43.59, 52.07, 54.72, 60.82, 61.69, 61.80, 110.64, 120.36, 122.23, 126.93, 126.97, 127.30, 128.58, 128.76, 129.35, 130.61, 136.42, 137.51, 141.95, 162.22, 169.24, 171.16, 171.78, 172.95 ppm. MS (ESI): m/z (%) = 627.3 $(M+H)^+$. IR (ATR): ν = 3279, 1731, 1647, 1513, 1448, 1375, 1334, 1199, 1122, 1027, 830, 743, 698 cm^{-1}. HPLC (254 nm): 96.8%, t_r = 21.99 min. HRMS Calcd for $C_{35}H_{39}N_4O_7$ m/z: 627.2819 $(M+H)^+$, found 627.2814. $[\alpha]_D^{20}$ = -13.1° (*c* 0.16, CH_2Cl_2).

4.3.8 Diethyl cinnamoylglycyl-L-phenylalanyl-D-glutamate **(11).** Synthesized according to the *General procedure for EDC-mediated coupling*. White amorphous solid, yield: 119 mg

(74%); m.p. 115-117 °C. ^{1}H-NMR ($CDCl_3$, 400 MHz): δ = 1.18-1.23 (m, 6H, 2 × $CH_2C\underline{H}_3$), 1.84-1.94 (m, 1H, <u>H</u>-β-Glu), 1.97-2.13 (m, 3H, <u>H</u>-β-Glu and $C\underline{H}_2$-γ-Glu), 3.10 (d, 2H, *J* = 7.2 Hz, $C\underline{H}_2$-Phe), 4.04-4.23 (m, 6H, 2 × $C\underline{H}_2CH_3$ and $NHC\underline{H}_2$), 4.52-4.57 (m, 1H, α-C<u>H</u>), 4.98-5.04 (m, 1H, α-C<u>H</u>), 6.63 (d, 1H, *J* = 16.0 Hz, CH=C<u>H</u>), 7.13-7.22 (m, 5H, Ar-<u>H</u>), 7.33-7.35 (m, 3H, Ar-<u>H</u> and $CON\underline{H}CH_2$), 7.49-7.51 (m, 2H, Ar-<u>H</u> and N<u>H</u>), 7.59–7.67 (m, 2H, C<u>H</u>=CH in NH) ppm. ^{13}C-NMR ($CDCl_3$, 100 MHz): δ = 14.09, 14.19, 26.87, 30.01, 39.04, 43.51, 51.70, 54.49, 60.62, 61.58, 120.33, 126.96, 127.94, 128.59, 128.82, 129.42, 129.74, 134.90, 136.35, 141.53, 166.55, 169.15, 170.93, 171.50, 172.68 ppm. MS (ESI): m/z (%) = 538.3 $(M+H)^+$. IR (ATR): ν = 3258, 1734, 1691, 1645, 1612, 1552, 1523, 1450, 1392, 1328, 1254, 1195, 1106, 1075, 1033, 989, 774, 732, 695, 671, 622 cm^{-1}. HPLC (254 nm): 99.0%, t_r = 15.66 min. HRMS Calcd for $C_{29}H_{36}N_3O_7$ m/z: 538.2553 $(M+H)^+$, found 538.2560. $[\alpha]_D^{20}$ = -9.6° (*c* 0.15, CH_2Cl_2).

4.3.9 Diethyl (trans-2-phenylcyclopropane-1-carbonyl)glycyl-L-phenylalanyl-D-glutamate **(12).** Synthesized according to the *General procedure for EDC-mediated coupling*. White amorphous solid, yield: 98 mg (59%); m.p. 107-108 °C. ^{1}H-NMR ($CDCl_3$, 400 MHz): δ = 1.23–1.27 (m, 6H, 2 × $CH_2C\underline{H}_3$), 1.56–1.62 (m, 1H, PhCHC$\underline{H}_{2A}$CH), 1.69–1.75 (m, 1H, PhCHC$\underline{H}_{2B}$CH), 1.80–1.90 (m, 1H, $C\underline{H}_{2A}$-β-Glu), 1.97–2.06 (m, 1H, $C\underline{H}_{2B}$-β-Glu), 2.08–2.21 (m, 2H, $C\underline{H}_2$-γ-Glu), 2.45–2.51 (m, 1H, PhC<u>H</u>CH_2CH), 3.03–3.13 (m, 2H, $C\underline{H}_2$-Phe), 3.88–4.04 (m, 2H, $NHC\underline{H}_2$), 4.06–4.17 (m, 4H, 2 x $C\underline{H}_2CH_3$), 4.43–4.48 (m, 1H, α-C<u>H</u>), 4.77 (q, 1H, *J* = 7.2 Hz, α-C<u>H</u>), 6.64 (s, 1H, <u>H</u>-Ar), 6.77–6.81 (m, 1H, <u>H</u>-Ar), 6.90 (t, 1H, *J* = 7.2 Hz, NH), 7.07–7.09 (m, 2H, <u>H</u>-Ar), 7.18–7.29 (m, 6H, 4 × <u>H</u>-Ar and 2 × N<u>H</u>) ppm. ^{13}C-NMR ($CDCl_3$, 100 MHz): δ = 14.13, 14.19, 16.28, 25.43, 26.13, 26.7730.07, 38.38, 43.57, 51.84, 54.33, 60.76, 61.67, 126.09, 126.38, 127.12, 128.47, 128.73, 129.30, 136.23, 140.40, 168.86, 170.53, 171.44, 172.68, 172.86, 172.89 ppm. MS (ESI): m/z (%) = 552.3 $(M+H)^+$. IR (ATR):

ν = 3273, 1729, 1628, 1525, 1498, 1445, 1377, 1267, 1179, 1114, 1026, 743, 697 cm^{-1}. HPLC (254 nm): 100.0%, t_r = 16.93 min (mixture of 2 diastereomers). HRMS Calcd for $C_{30}H_{38}N_3O_7$ m/z: 552.2710 $(M+H)^+$, found 552.2714. $[\alpha]_D^{20}$ = +6.6° (*c* 0.14, CH_2Cl_2).

4.3.10 Diethyl ((E)-3-(3,4-difluorophenyl)acryloyl)glycyl-L-phenylalanyl-D-glutamate **(13).** Synthesized according to the *General procedure for EDC-mediated coupling*. White amorphous solid, yield: 131 mg (76%); m.p. 122-124 °C. ^{1}H-NMR ($CDCl_3$, 400 MHz): δ = 1.18–1.25 (m, 6H, 2 × CH_2CH_3), 1.83–1.93 (m, 1H, CH_2-β-Glu), 1.97–2.17 (m, 3H, CH_2-β-Glu and CH_2-γ-Glu), 3.09 (d, *J* = 7.2 Hz, CH_2-Phe), 4.03–4.25 (m, 5H, 2 × CH_2CH_3 and NH-CH_{2A}), 4.20–4.25 (m, 1H, NH-CH_{2B}), 4.49–4.54 (m, 1H, α-CH), 5.00 (q, 1H, *J* = 7.2 Hz, α-CH), 6.55 (d, 1H, *J* = 15.6 Hz, CH=CH), 7.11–7.24 (m, 6H, H-Ar), 7.33–7.38 (m, 2H, H-Ar), 7.52–7.56 (m, 2H, NH and CH=CH), 7.61 (d, 1H, *J* = 7.6 Hz, NH) ppm. ^{13}C-NMR ($CDCl_3$, 100 MHz): δ = 14.07, 14.17, 26.86, 29.99, 39.07, 43.44, 51.74, 54.49, 60.69, 61.64, 116.18 (d, *J* = 17.5 Hz), 117.70 (d, *J* = 17.3 Hz), 121.32 (d, *J* = 2.5 Hz), 124.64, 127.02, 128.61, 129.38, 136.27, 139.36, 144.94 (d, *J* = 109.5 Hz), 145.45 (d, *J* = 93.4 Hz), 165.96, 168.95, 170.87, 171.52, 172.69 ppm. MS (ESI): m/z (%) = 574.2 $(M+H)^+$. IR (ATR): ν = 3305, 1735, 1647, 1608, 1514, 1434, 1375, 1334, 1297, 1273, 1184, 1114, 1024, 985, 968, 858, 823, 777, 739, 697, 647 cm^{-1}. HPLC (254 nm): 99.2%, t_r = 17.25 min. HRMS Calcd for $C_{29}H_{34}F_2N_3O_7$ m/z: 574.2365 $(M+H)^+$, found 574.2360. $[\alpha]_D^{20}$ = -17.7° (*c* 0.12, CH_2Cl_2).

4.3.11 Diethyl (2-(3,4-difluorophenyl)cyclopropane-1-carbonyl)glycyl-L-phenylalanyl-D-glutamate **(14).** Synthesized according to the *General procedure for EDC-mediated coupling*. White amorphous solid, yield: 92 mg (52%); m.p. 89-92 °C. ^{1}H-NMR ($CDCl_3$, 400 MHz): δ = 1.15–1.27 (m, 7H, 2 × CH_2CH_3 and PhCHCH_{2A}CH), 1.51–1.57 (m, 1H, PhCHCH_{2B}CH), 1.74–1.87 (m, 2H, PhCHCH_2CH and CH_{2A}-β-Glu), 1.90–2.08 (m, 3H, CH_{2B}-β-Glu and CH_2-

γ-Glu), 2.38-2.49 (m, 1H, PhCHCH$_2$CH), 2.99-3.10 (m, 2H, PhCH$_2$), 3.95–4.17 (m, 6H, NHCH$_2$ and 2 × CH$_2$CH$_3$), 4.40–4.46 (m, 1H, α-CH), 4.90–4.97 (m, 1H, α-CH), 6.82–6.84 (m, 1H, H-Ar), 6.87–6.92 (m, 1H, H-Ar), 7.00–7.06 (m, 1H, H-Ar), 7.15–7.26 (m, 6H, 5 × H-Ar and NH), 7.33–7.44 (m, 2H, 2×NH) ppm. ^{13}C-NMR ($CDCl_3$, 100 MHz): δ = 14.07, 14.19, 16.02, 24.27, 24.34, 24.94, 25.67, 26.85, 29.92, 33.92?, 39.13, 42.65?, 43.43, 51.61, 54.36, 60.71, 61.65, 115.13 (d, *J* = 18.2 Hz), 117.11 (d, *J* = 17.0 Hz), 122.37, 127.05, 128.59, 129.37, 136.19, 137.83, 148.36 (dd, *J* = 127.0 Hz, *J* = 12.5 Hz), 150.77 (dd, *J* = 117.6 Hz, *J* = 10.2 Hz), 168.82, 170.73, 171.48, 172.21, 172.65 ppm. MS (ESI): m/z (%) = 588.3 $(M+H)^+$. IR (ATR): ν = 3283, 1735, 1646, 1518, 1436, 1376, 1334, 1273, 1192, 1115, 1024, 858, 819, 776, 741, 698 cm^{-1}. HPLC (254 nm): 17.4% (t_r = 17.25 min), 82.6% (t_r = 18.41 min); total: 100.0% (mixture of 4 diastereomers). HRMS Calcd for $C_{30}H_{36}F_2N_3O_7$ m/z: 588.2521 $(M+H)^+$, found 588.2526. $[\alpha]_D^{20}$ = +29.1° (*c* 0.20, CH_2Cl_2).

4.3.12 Diethyl ((E)-3-(4-hydroxy-3-methoxyphenyl)acryloyl)glycyl-L-phenylalanyl-D-glutamate **(15).** Synthesized according to the *General procedure for EDC-mediated coupling*. Yellow-white amorphous solid, yield: 84 mg (48%); m.p. 70-73 °C. ^{1}H-NMR ($CDCl_3$, 400 MHz): δ = 1.18–1.22 (m, 6H, 2 × CH$_2$CH$_3$), 1.83–1.93 (m, 1H, CH$_{2A}$-β-Glu), 1.98–2.06 (m, 1H, CH$_{2B}$-β-Glu), 2.09–2.14 (m, 2H, CH$_2$-γ-Glu), 3.02–3.14 (m, 2H, CH$_2$-Phe), 3.83 (s, 3H, OCH_3), 4.03–4.13 (m, 6H, 2 × CH$_2$CH$_3$ and NHCH$_2$), 4.47–4.52 (m, 1H, α-CH), 4.86–4.92 (m, 1H, α-CH), 6.36 (d, 1H, *J* = 15.6 Hz, CH=CHCO), 6.85 (d, 1H, *J* = 8.0 Hz, H-Ar), 6.92–7.23 (m, 8H, 6 × H-Ar and NHCH$_2$ and NH), 7.46–7.66 (m, 3H, CH=CHCO and NH and H-Ar) ppm. ^{13}C-NMR ($CDCl_3$, 100 MHz): δ = 14.09, 14.18, 26.77, 30.06, 38.56, 43.48, 51.82, 54.58, 55.92, 55.96, 60.67, 61.66, 110.24, 114.90, 117.56, 122.08, 126.94, 127.24, 128.60, 129.35, 136.48, 141.72, 146.90, 147.08, 147.62, 167.02, 169.48, 171.12, 171.73, 172.75 ppm. MS (ESI): m/z (%) = 584.3 $(M+H)^+$. IR (ATR): ν = 3279, 1729, 1649, 1509, 1452, 1376,

1257, 1197, 1120, 1028, 980, 846, 815, 700 cm^{-1}. HPLC (254 nm): 96.5%, t_r = 11.34 min. HRMS Calcd for $C_{26}H_{36}N_3O_9$ m/z: 584.2608 $(M+H)^+$, found 584.2605. $[\alpha]_D^{20}$ = -14.8° (*c* 0.15, CH_2Cl_2).

4.3.13 Diethyl ((E)-3-(4-hydroxy-3-methoxyphenyl)acryloyl)glycyl-L-alanyl-D-glutamate **(16).** Synthesized according to the *General procedure for EDC-mediated coupling*. White amorphous solid, yield: 66 mg (43%); m.p. 86-89 °C. ^{1}H-NMR ($CDCl_3$, 400 MHz): δ = 1.21–1.28 (m, 6H, 2 × $CH_2C\underline{H}_3$), 1.42 (d, 3H, *J* = 7.2 Hz, $C\underline{H}_3$-Ala) 1.99–2.08 (m, 1H, $C\underline{H}_{2A}$-β-Glu), 2.17–2.25 (m, 1H, $C\underline{H}_{2B}$-β-Glu), 2.33–2.45 (m, 2H, $C\underline{H}_2$-γ-Glu), 3.91 (s, 3H, OCH_3), 4.00–4.22 (m, 6H, 2 × $C\underline{H}_2CH_3$ and $NHC\underline{H}_2$), 4.51–4.62 (m, 1H, α-CH-Glu and α-CH-Ala), 5.91 (br s, 1H, OH), 6.33 (d, 1H, *J* = 15.6 Hz, CH=C<u>H</u>), 6.61 (t, 1H, *J* = 5.2 Hz, N<u>H</u>CH_2), 6.88–6.92 (m, 2H, <u>H</u>-Ar and N<u>H</u>), 7.01 (d, 1H, *J* = 1.2 Hz, <u>H</u>-Ar), 7.06 (dd, 1H, *J* = 8.4 Hz, *J* = 1.5 Hz, <u>H</u>-Ar), 7.18 (d, 1H, *J* = 7.6 Hz, N<u>H</u>), 7.54 (d, 1H, *J* = 15.6 Hz, CH=C<u>H</u>) ppm. ^{13}C-NMR ($CDCl_3$, 100 MHz): δ = 14.13, 14.16, 18.10, 26.74, 30.38, 43.61, 48.94, 51.99, 55.95, 60.86, 61.75, 109.70, 122.42, 127.12, 146.72, 147.62, 162.92, 165.09, 169.08, 171.81, 172.13, 173.09, 173.25 ppm. MS (ESI): m/z (%) = 508.2 $(M+H)^+$. IR (ATR): ν = 3297, 1730, 1641, 1603, 1515, 1448, 1376, 1268, 1192, 1120, 1021, 977, 845, 813, 637 cm^{-1}. HPLC (254 nm): 95.8%, t_r = 4.95 min. HRMS Calcd for $C_{24}H_{34}N_3O_9$ m/z: 508.2295 $(M-H)^-$, found 508.2281. $[\alpha]_D^{20}$ = +3.0° (*c* 0.09, CH_2Cl_2).

4.3.14 ((E)-3-(4-hydroxy-3-methoxyphenyl)acryloyl)glycyl-L-valyl-D-glutamic acid **(17).** Synthesized from **9** according to the *General procedure for alkaline hydrolysis*. Ochre amorphous solid, yield: 21 mg (86%); m.p. 100-104 °C. ^{1}H-NMR (DMSO-d_6, 400 MHz): δ = 0.83 (d, 3H, *J* = 6.8 Hz, $C\underline{H}_3$-Val), 0.85 (d, 3H, *J* = 6.8 Hz, $C\underline{H}_3$-Val), 1.73–1.83 (m, 1H, $C\underline{H}_{2A}$-β-Glu), 1.91–2.01 (m, 2H, $C\underline{H}_{2B}$-β-Glu and $C\underline{H}(CH_3)_2$), 2.26 (t, 2H, *J* = 7.6 Hz, $C\underline{H}_2$-γ-

Glu), 3.80 (s, 3H, OCH_3), 3.88 (d, 2H, J = 5.6 Hz, $NHCH_2$), 4.20–4.30 (m, 2H, α-CH-Glu and α-CH-Val), 6.56 (d, 1H, J = 15.6 Hz, CH=CH), 6.79 (d, 1H, J = 8.0 Hz, H-Ar), 7.00 (dd, 1H, J = 8.4 Hz, J = 1.5 Hz, H-Ar), 7.14 (d, 1H, J = 1.2 Hz, H-Ar), 7.32 (d, 1H, J = 15.6 Hz, CH=CH), 7.87 (d, 1H, J = 8.8 Hz, NH), 8.19 (t, 1H, J = 5.6 Hz, $NHCH_2$), 8.29 (d, 1H, J = 7.6 Hz, NH), 9.45 (s, 1H, OH) ppm. ^{13}C-NMR (DMSO-d_6, 100 MHz): δ = 17.69, 19.10, 29.88, 55.47, 123.64, 124.69, 127.77, 139.00, 147.77, 170.87, 173.15, 173.69 ppm. MS (ESI): m/z (%) = 480.2 $(M+H)^+$. IR (ATR): ν = 3292, 2924, 1648, 1513, 1429, 1371, 1204, 1125, 1030, 979, 845, 815 cm^{-1}. HPLC (254 nm): 100%, t_r = 2.14 min. HRMS Calcd for $C_{22}H_{30}N_3O_9$ m/z: 480.1982 $(M+H)^+$, found 480.1986. $[\alpha]_D^{20}$ = +8.8° (*c* 0.25, CH_2Cl_2).

4.3.15 Ethyl (E)-1-((E)-(3-(4-hydroxy-3-methoxyphenyl)acryloyl)glycyl-L-valyl)piperidine-4-carboxylate **(22).** Synthesized according to the *General procedure for EDC-mediated coupling*. White amorphous solid, yield: 92 mg (63%); m.p. 90-94 °C. ^{1}H-NMR ($CDCl_3$, 400 MHz): δ = 0.85–0.94 (m, 6H, 2 × CH_3-Val), 1.23 (t, 3H, J = 7.6 Hz, OCH_2CH_3), 1.52–1.77 (m, 2H, NCH_2CH_2), 1.89–2.00 (m, 3H, NCH_2CH_2 in CHCOO), 2.49–2.54 (m, 1H, $CH(CH_3)_2$), 2.86 (t, 1H, J = 10.8 Hz, NCH_2CH_2), 3.17 (t, 1H, J = 12.0 Hz, NCH_2CH_2), 3.80 (s, 3H, OCH_3), 3.93–3.99 (m, 1H, $NHCH_2$), 4.07–4.15 (m, 2H, OCH_2CH_3), 4.31–4.39 (m, 1H, $NHCH_2$), 4.81–4.85 (m, 1H, α-CH), 6.28 (d, 1H, J = 15.6 Hz, CH=CH), 6.81–6.94 (m, 3H, 2 × H-Ar), 7.04–7.10 (t, 1H, J = Hz, $NHCH_2$), 7.32–7.39 (m, 1H, NH), 7.48 (dd, 1H, J = 15.6 Hz, J = 3.2 Hz, CH=CH) ppm. ^{13}C-NMR ($CDCl_3$, 100 MHz): δ = 14.18, 17.45, 17.49, 19.63, 19.75, 27.72, 27.92, 28.41, 28.56, 30.96, 31.49, 31.51, 40.64, 40.87, 41.49, 41.62, 43.11, 43.49, 45.06, 45.37, 53.56, 53.61, 55.89, 60.75, 109.99, 114.92, 117.44, 122.22, 122.27, 127.13, 127.16, 141.57, 146.93, 147.65, 166.73, 169.22, 169.36, 169.92, 169.99, 173.87, 174.08 ppm*. MS (ESI): m/z (%) = 490.3 $(M+H)^+$. IR (ATR): ν = 3293, 2964, 1725, 1619, 1513, 1449, 1372, 1270, 1179, 1123, 1035, 979, 846, 817, 635 cm^{-1}. HPLC (254 nm): 97.5%,

t_r = 7.04 min. HRMS Calcd for $C_{25}H_{36}N_3O_7$ m/z: 490.2553 $(M+H)^+$, found 490.2561. $[\alpha]_D^{20}$ = +21.9° (*c* 0.08, CH_2Cl_2). *(doubling of peaks is observed as this compound is a mixture of two diastereomers)

4.3.16 Ethyl (1R,2S)-2-((S)-2-(2-((E)-3-(4-hydroxy-3-methoxyphenyl)acrylamido)acetamido)-3-methylbutanamido)cyclohexane-1-carboxylate **(23).** Synthesized according to the *General procedure for EDC-mediated coupling*. White amorphous solid, yield: 115 mg (76%); m.p. 93-97 °C. ^{1}H-NMR ($CDCl_3$, 400 MHz): δ = 0.85–0.95 (m, 6H, 2 × C<u>H</u>$_3$-Val), 1.18–1.26 (m, 3H, OCH$_2$C<u>H</u>$_3$), 1.28–1.42 (m, 3H, C<u>H</u>$_2$ and C<u>H</u>$_{2A}$), 1.55–1.65 (m, 3H, C<u>H</u>$_2$ and C<u>H</u>$_{2B}$), 1.72–1.87 (m, 1H, C<u>H</u>(CH$_3$)$_2$), 1.95–2.13 (m, 2H, C<u>H</u>$_2$), 2.70–2.78 (m, 1H, C<u>H</u>COO), 3.85 (s, 3H, OC<u>H</u>$_3$), 4.03–4.24 (m, 5H, OC<u>H</u>$_2$CH$_3$, NHC<u>H</u>$_2$ and NHC<u>H</u>), 4.30–4.42 (m, 1H, α-CH), 6.36–6.43 (m, 1H, C<u>H</u>=CH), 6.86 (dd, 1H, *J* = 8.0 Hz, J = 2.0 Hz, <u>H</u>-Ar), 6.96 (s, 1H, <u>H</u>-Ar), 7.00–7.02 (m, 1H, N<u>H</u>CH$_2$), 7.12–7.15 (m, 1H, <u>H</u>-Ar), 7.28–7.33 (m, 1H, *J* = 8.4 Hz, N<u>H</u>), 7.56 (dd, 1H, *J* = 15.6 Hz, J = 6.0 Hz, C<u>H</u>=CH) ppm. ^{13}C-NMR ($CDCl_3$, 100 MHz): δ = 14.15, 14.17, 18.04, 18.23, 19.14, 22.64, 29.17, 29.57, 31.36, 31.44, 43.39, 44.25, 44.31, 47.89, 55.91, 58.66, 58.72, 60.55, 60.65, 109.96, 110.02, 114.85, 117.55, 117.64, 122.09, 122.16, 127.26, 127.31, 141.61, 141.66, 146.84, 147.59, 166.75, 166.81, 169.32, 169.39, 170.07, 170.23, 173.92, 174.00 ppm*. MS (ESI): m/z (%) = 504.3 $(M+H)^+$. IR (ATR): ν = 3275, 2939, 2360, 2341, 1646, 1515, 1449, 1374, 1251, 1124, 1032, 983, 669 cm^{-1}. HPLC (254 nm): 98.7%, t_r = 8.85 (and 9.25)* min. HRMS Calcd for $C_{26}H_{38}N_3O_7$ m/z: 504.2717 $(M+H)^+$, found 504.2710. $[\alpha]_D^{20}$ = -17.0° (*c* 0.07, CH_2Cl_2).*(doubling of certain peaks is observed as this compound is a mixture of two diastereomers)

4.3.17 Ethyl (1S,2S)-2-((S)-2-(2-((E)-3-(4-hydroxy-3-methoxyphenyl)acrylamido)acetamido)-3-methylbutanamido)cyclohexane-1-carboxylate **(24).** Synthesized according to the *General*

procedure for EDC-mediated coupling. White amorphous solid, yield: 131 mg (87%); m.p. 108-112 °C. ^{1}H-NMR (MeOD, 400 MHz): δ = 0.92–0.97 (m, 6H, 2 × C$\underline{H}_3$-Val), 1.19–1.40 (m, 6H, OCH$_2$C$\underline{H}_3$, C$\underline{H}_2$ and C$\underline{H}_{2A}$), 1.47–1.56 (m, 1H, C$\underline{H}_{2B}$), 1.75–1.77 (m, 2H, C$\underline{H}_2$), 1.84–2.13 (m, 3H, CH$_2$, C$\underline{H}$(CH$_3$)$_2$), 2.39–2.52 (m, 1H, C$\underline{H}$COO), 3.86–4.18 (m, 9H, OC$\underline{H}_3$, OC$\underline{H}_2$CH$_3$, NHC$\underline{H}_2$, NHC$\underline{H}$ and α-CH), 6.53 (dd, 1H, *J* = 15.8 Hz, *J* = 0.8 Hz, C$\underline{H}$=CH), 6.82 (dd, 1H, *J* = 8.0 Hz, *J* = 1.6 Hz, $\underline{H}$-Ar), 7.06 (dd, 1H, *J* = 8.8 Hz, *J* = 0.8 Hz, $\underline{H}$-Ar), 7.16 (t, 1H, *J* = 1.6 Hz, $\underline{H}$-Ar), 7.51 (dd, 1H, *J* = 15.6 Hz, *J* = 6.0 Hz, C$\underline{H}$=CH) ppm. ^{13}C-NMR (MeOD, 100 MHz): δ = 14.50, 14.57, 18.33, 18.41, 19.70, 19.74, 25.72, 25.87, 30.30, 30.52, 32.00, 32.24, 33.22, 33.40, 43.82, 44.01, 50.22, 50.39, 50.91, 50.98, 56.41, 60.15, 60.24, 61.72, 61.76, 111.59, 116.51, 118.06, 118.12, 123.45, 128.13, 142.87, 142.94, 149.33, 150.08, 169.62, 171.58, 171.74, 172.42, 175.83, 175.86 ppm*. MS (ESI): m/z (%) = 504.3 (M+H)$^+$. IR (ATR): ν = 3276, 2937, 2360, 2342, 1725, 1645, 1513, 1449, 1374, 1268, 1124, 1031, 979, 845, 812, 669 cm^{-1}. HPLC (254 nm): 96.3%, t_r = 7.04 (and 7.94)* min. HRMS Calcd for $C_{26}H_{38}N_3O_7$ m/z: 504.2715 (M+H)$^+$, found 504.2710. $[\alpha]_D^{20}$ = -39.9° (*c* 0.18, CH_2Cl_2). *(doubling of certain peaks is observed as this compound is a mixture of two diastereomers)

4.3.18 Ethyl (S,E)-5-hydroxy-2-(2-(2-(3-(4-hydroxy-3-methoxyphenyl)acrylamido)acetamido)-3-methylbutanamido)benzoate **(28).** Synthesized according to the *General procedure for EDC-mediated coupling*. White amorphous solid, yield: 86 mg (56%); m.p. 116-120 °C. ^{1}H-NMR (MeOD, 400 MHz): δ = 0.96–1.00 (m, 6H, 2 × C$\underline{H}_3$-Val), 1.32 (t, 3H, *J* = 7.2 Hz, OCH$_2$C$\underline{H}_3$), 2.27–2.36 (m, 1H, C$\underline{H}$(CH$_3$)$_2$), 3.83 (s, 3H, OC$\underline{H}_3$), 4.18 (s, 2H, NHC$\underline{H}_2$), 4.28–4.35 (m, 3H, OC$\underline{H}_2$CH$_3$ and α-CH), 6.48 (d, 1H, *J* = 15.6 Hz, C$\underline{H}$=CH), 6.74 (d, 1H, *J* = 8.4 Hz, $\underline{H}$-Ar), 6.95–7.00 (m, 2H, 2 × $\underline{H}$-Ar), 7.08 (d, 1H, *J* = 2.0 Hz, $\underline{H}$-Ar), 7.39 (d, 1H, *J* = 3.2 Hz, $\underline{H}$-Ar), 7.43 (d, 1H, *J* = 15.6 Hz, C$\underline{H}$=CH), 8.30 (d, 1H, *J* = 9.2 Hz, $\underline{H}$-Ar) ppm. ^{13}C-NMR (MeOD, 100 MHz): δ = 14.47, 18.07, 19.84, 31.29, 43.80, 56.38, 61.75, 62.77, 111.57,

116.47, 117.59, 118.20, 119.25, 122.21, 123.38, 123.42, 128.14, 133.65, 142.76, 149.30, 150.02, 154.53, 169.12, 169.57, 171.63, 172.51 ppm. MS (ESI): m/z (%) = 514.2 $(M+H)^+$. IR (ATR): ν = 3286, 2361, 2342, 1652, 1589, 1513, 1436, 1229, 1123, 1078, 1028, 977, 820, 787, 754, 669, 609 cm^{-1}. HPLC (254 nm): 96.3%, t_r = 8.02 min. HRMS Calcd for $C_{26}H_{32}N_3O_8$ m/z: 514.2189 $(M+H)^+$, found 514.2178. $[\alpha]_D^{20}$ = +43.9° (*c* 0.09, CH_2Cl_2).

4.3.19 Dimethyl (S,E)-5-(2-(2-(3-(4-hydroxy-3-methoxyphenyl)acrylamido)acetamido)-3-methylbutanamido)isophthalate **(29).** Synthesized according to the *General procedure for EDC-mediated coupling*. White amorphous solid, yield: 119 mg (73%); m.p. 122-126 °C. ^{1}H-NMR ($CDCl_3$, 400 MHz): δ = 0.97–1.25 (m, 6H, 2 × C<u>H</u>$_3$-Val), 2.21–2.33 (m, 1H, C<u>H</u>$(CH_3)_2$), 3.77 (s, 3H, OC<u>H</u>$_3$), 3.84 (s, 6H, 2 × OC<u>H</u>$_3$), 4.22–4.27 (m, 1H, NHC<u>H</u>$_{2A}$), 4.37–4.42 (m, 1H, NHC<u>H</u>$_{2B}$), 4.79–4.83 (m, 1H, α-CH), 6.52 (d, 1H, *J* = 16.0 Hz, C<u>H</u>=CH), 6.76 (d, 1H, *J* = 8.0 Hz, N<u>H</u>), 6.90–6.97 (m, 2H, 2 x <u>H</u>-Ar), 7.61 (d, 1H, *J* = 16.4 Hz, C<u>H</u>=CH), 7.68 (s, 1H, <u>H</u>-Ar), 7.81 (d, 1H, *J* = 8.8 Hz, N<u>H</u>), 8.35 (s, 1H, <u>H</u>-Ar), 8.57–8.59 (m, 2H, 2 x <u>H</u>-Ar), 9.96 (s, 1H, N<u>H</u>-Ar) ppm. ^{13}C-NMR ($CDCl_3$, 100 MHz): δ = 18.53, 19.28, 28.05, 32.01, 52.42, 55.71, 59.27, 110.27, 114.64, 117.69, 121.73, 125.12, 126.23, 127.31, 131.13, 131.25, 138.62, 141.68, 146.58, 147.36, 165.80, 165.93, 167.39, 169.91, 170.66 ppm. MS (ESI): m/z (%) = 542.2 $(M+H)^+$. IR (ATR): ν = 3276, 2361, 1725, 1651, 1601, 1513, 1436, 1340, 1244, 1123, 1031, 812, 756, 721, 669 cm^{-1}. HPLC (254 nm): 94.7%, t_r = 10.67 min. HRMS Calcd for $C_{27}H_{32}N_3O_9$ m/z: 542.2139 $(M+H)^+$, found 542.2128. $[\alpha]_D^{20}$ = -23.1° (*c* 0.26, CH_2Cl_2).

4.3.20 Dimethyl (S,E)-2-(2-(2-(3-(4-hydroxy-3-methoxyphenyl)acrylamido)acetamido)-3-methylbutanamido)terephthalate **(30).** Synthesized according to the *General procedure for EDC-mediated coupling*. White amorphous solid, yield: 44 mg (27%); m.p. 109-113 °C. ^{1}H-

NMR ($CDCl_3$, 400 MHz): δ = 1.00–1.04 (m, 6H, 2 × C<u>H</u>$_3$-Val), 2.36–2.44 (m, 1H, C<u>H</u>$(CH_3)_2$), 3.85 (s, 3H, OC<u>H</u>$_3$), 3.88 (s, 3H, OC<u>H</u>$_3$), 3.90 (s, 3H, OC<u>H</u>$_3$), 4.27–4.38 (m, 1H, NHC<u>H</u>$_2$), 4.52–4.56 (m, 1H, α-CH), 6.32 (d, 1H, *J* = 15.6 Hz, C<u>H</u>=CH), 6.83 (d, 1H, *J* = 8.0 Hz, <u>H</u>-Ar), 6.92–6.96 (m, 2H, H-Ar), 7.07–7.09 (m, 1H, N<u>H</u>CH_2), 7.50 (d, 1H, J = 15.6 Hz, C<u>H</u>=CH), 7.59 (d, 1H, *J* = 7.6 Hz, N<u>H</u>), 7.68 (dd, 1H, *J* = 8.0 Hz, *J* = 2.0 Hz, <u>H</u>-Ar), 7.98 (d, 1H, *J* = 8.8 Hz, <u>H</u>-Ar), 9.31 (s, 1H, OH), 11.44 (s, 1H, N<u>H</u>-Ar) ppm. ^{13}C-NMR ($CDCl_3$, 100 MHz): δ = 17.66, 19.45, 30.68, 43.82, 52.61, 52.81, 55.92, 60.08, 109.58, 114.70, 117.22, 118.33, 121.11, 122.40, 123.59, 127.05, 130.91, 135.31, 140.76, 141.87, 146.73, 147.61, 166.01, 166.93, 167.99, 170.06, 170.28 ppm. MS (ESI): m/z (%) = 542.2 $(M+H)^+$. IR (ATR): ν = 3287, 2361, 2341, 1647, 1582, 1514, 1418, 1247, 1110, 1082, 1030, 984, 848, 811, 754, 669 cm^{-1}. HPLC (254 nm): 96.7%, t_r = 12.11 min. HRMS Calcd for $C_{27}H_{32}N_3O_9$ m/z: 542.2139 $(M+H)^+$, found 542.2129. $[\alpha]_D^{20}$ = -28.5° (*c* 0.24, CH_2Cl_2).

4.4 Cell culture

Human PBMC from healthy blood donors were isolated by density gradient centrifugation with Ficoll-Paque (Pharmacia, Sweden). The cells were cultured in RPMI 1640 (Sigma, Germany) supplemented with 100 U/mL penicillin (Sigma), 100 μg/mL streptomycin (Sigma), 2 mM L-glutamine (Sigma), 50 μM 2-mercaptoethanol (Sigma) and 10% heat-inactivated foetal bovine serum (Gibco, USA). 1×10^6 cells were plated on 24-well culture plates (Nunc, Denmark) and cultivated at 37 °C in a humidified atmosphere of 5% CO_2 in air.

4.5 Cytotoxicity assay

HEK-Blue NOD2 cells (Invivogen, San Diego/CA, USA) were cultured in accordance with the manufacturer's instructions. HEK-Blue NOD2 cells ($1x10^5$ cells/mL) were treated with the appropriate amounts of compounds or with the corresponding vehicle (control cells), then

seeded in duplicate in 96 well plates. After 18 h metabolic activity was assessed using the CellTiter 96® Aqueous One Solution Cell Proliferation Assay (Promega, Madison/WI, USA), in accordance with the manufacturer's instructions. The results are expressed as means of duplicates ± S.E.M. of three independent experiments.

4.6 Measurement of NF-κB transcriptional activity (Quanti-blue assay)

HEK-Blue NOD2 cells and NOD1 cells (Invivogen, San Diego/CA, USA) were cultured in accordance with the manufacturer's instructions. HEK-Blue NOD2 cells and NOD1 cells, were assayed for changes in NF-κB transcriptional activity upon incubation (5×10^5 cells/mL) with MDP and other NOD2 agonistic compounds (2 and 20 μM) for 18 h. Secreted embryonic alkaline phosphatase (SEAP) activity was determined in the supernatant in accordance with the manufacturer's instructions. Absorbance was measured on a BioTek Synergy microplate reader (VT, USA) at 640 nm. The results are expressed as means of duplicates ± S.E.M. of three independent experiments.

4.7 Multiplexed cytokine assays

PBMCs were treated with MDP or the compound of interest in the presence or absence of 10 ng/mL LPS. Cell-free supernatants were collected at 18 h and stored at -78 °C before being evaluated for cytokines by a commercially available kit. Cytokine production was assessed by BD Cytometric Bead Array (CBA) Human Th1/Th2/Th17 Kit (Content: IL-2, IL-4, IL-6, IL-10, TNF-α, IFNγ, IL-17A). Flow cytometric analyses were performed using a FACSCalibur flow cytometer with Sorting Option: 4-Color and CELLQuest software (BD Biosciences; San Diego, CA, USA). Standard curves were generated using recombinant cytokines provided in the kit. The data were analyzed with FlowJo software (Tree Star, Inc., Ashland, OR). Results

are expressed in pg/mL. The results are expressed as means of duplicates ± S.E.M. of two independent experiments.

4.8. Preparation of liposomes

Multilamellar liposomes were prepared by the modified thin lipid film method following previously described methods.[76,77] Egg-phosphatidylcholine, cholesterol and dicetylphosphate (total mass of lipid was 4 mg/mL in a molar ratio of 7:5:1) were dissolved in chloroform:methanol (2:1). For incorporation of MDP or compound **9** in liposomes, the lipid solution was mixed with a solution of MDP or compound **9** in methanol or chloroform:methanol. After rotary evaporation of the solvent the remaining lipid film was dried in vacuum for an hour and then dispersed by gentle hand shaking in 0.1 mg/mL OVA solution in saline. The concentration of MDP and compound **9** in the liposome suspension was 2 mM. The latter was left overnight at 4 °C to swell and stabilize. Liposome size was reduced by sequential extrusion of the multilamellar vesicles through polycarbonate membranes of 800 and 200 nm using the 0.5 mL extruder (LiposoFast, Avestin Inc., Canada). Non-entrapped material was not separated from liposome and the complete liposome suspension was used for immunizations.

4.9 Materials, antigen and antibodies

Bovine serum albumin (BSA), Tween 20, tris(hydroxymethyl)aminomethane, monoclonal anti-chicken egg albumin (clone OVA-14 mouse IgG1 isotype), *o*-phenylenediamine dihydrochloride (OPD), MDP and avidin–peroxidase were from Sigma, USA. Horseradish peroxidase conjugated goat anti-mouse IgG (HRP-anti-mouse IgG) was from Bio-Rad Laboratories, USA. Biotin-conjugated rat anti-mouse IgG1 and anti-mouse IgG2a monoclonal antibodies and streptavidin–peroxidase were purchased from PharMingen, Becton Dickinson

(USA). Chemicals for buffers and solutions were from Kemika, Croatia. Ovalbumin (OVA) was from Serva, Germany. L-α-phosphatidylcholine, type XI-E: from fresh egg yolk (egg-PC) were from Avanti Polar Lipids. Cholesterol from porcine liver (CHL) and dicetyl phosphate (DCPh) were purchased from Sigma (USA).

4.10 Experimental mice

NIH/OlaHsd inbred mice were raised at the Institute of Immunology, Croatia. All mice used were females from 2 to 2.5 months old. During the experimental period animals were housed in the Animal Facility of the Institute of Immunology. Commercial food and water were provided ad libitum. All animal work was performed according to the Croatian Law on Animal Welfare (NN 135/06).

4.11 Immunizations

Experimental groups of six female mice were immunized and boosted two times subcutaneously (s.c.) into the tail base at 28-day intervals. The doses used per mouse were: OVA 10 μg, MDP and compound **9** 100 μg. The amount of lipids administered to each mouse was 400 μg. The injection volume in all experimental groups was 0.1 mL per mouse. Mice were anaesthetized prior to blood collection from axillary's plexus on the seventh day after second booster. Individual sera from each animal were decomplemented at 56 °C for 30 min and then stored at -20 °C until tested.

4.12 ELISA for anti-OVA IgG

Microtiter plates, flat-bottomed high binding (Costar, USA), were coated with 100 μL of 15 μg/ml OVA solution in carbonate buffer, pH 9.6, and left overnight at room temperature (RT). Non-specific antibody binding was blocked by incubation with 0.5% (*w*/*v*) BSA in PBS-T

(0.05% (*v*/*v*) Tween 20 in PBS) buffer (200 μL per well) for 2 h at 37 °C. Mice sera to be tested and standard preparation (100 μL per well) were added in five serial dilutions, and left overnight at room temperature (RT). All samples were analysed in duplicates. Plates were washed and 100 μL/well of HRP-anti-mouse IgG (4000× diluted) was added and incubated for 2 h at 37 °C. After washing, the substrate solution consisting of 0.6 mg/mL OPD solution in citrate–phosphate buffer, pH 5.0, with 0.5 μL 30% H_2O_2 /mL was added (100 μL per well) and incubated for 30 min at RT in the dark. The enzyme reaction was stopped with 50 μL per well of 12.5% H_2SO_4 and absorbance at 492 nm (A_{492}) was measured using a microplate reader (Thermoscientific Fisher, Finland). All washings (three times after each step) utilized PBS-T buffer in microplate washer (Multiwash; Labsystems, Finland). The relative quantity of anti-OVA IgGs was calculated by parallel line assay, where each serum was compared to the standard preparation, monoclonal anti-chicken egg albumin, to which we voluntarily assigned 20000 arbitrary units per mL (AU/mL).

4.13 ELISA for anti-OVA IgG1 and IgG2a

For quantification of OVA specific immunoglobulin G subclass, IgG1 and IgG2a, plates were coated with OVA and incubated with sera samples as described above. After washing, biotinylated rat anti-mouse IgG1 0.05 μg/mL or biotinylated rat anti-mouse IgG2a 0.5 μg/mL was added, 100 μL to each well and incubated for 2 h at 37 °C. For IgG1 determination streptavidin–peroxidase (100000× diluted) and for IgG2a determination avidin–peroxidase (50000× diluted) were added (100 μL/well) and incubated for another 2 h at 37 °C. Plates were washed and the substrate solution of 100 μL per well was added and incubated for 30 min at RT in the dark as describe above. The enzymatic reaction was stopped with 12.5 % H_2SO_4 (50 μL/well) and A_{492} was measured using a microplate reader. The relative quantities of antibody isotypes were determined by parallel line assay using appropriate standard

preparations for anti-OVA IgG1 and anti-OVA IgG2a.[78] The monoclonal anti-OVA IgG1 was a standard for relative quantification of anti-OVA IgG1 to which 400,000 AU/mL was assigned, while polyclonal mouse serum containing high levels of anti-OVA IgG2a was used as a standard for relative quantification of IgG2a specific antibodies with voluntarily assigned 5,000 AU/mL. The ratio of anti-OVA IgG1 and anti-OVA IgG2a (IgG1/IgG2a) was used as an indication of the Th1/Th2-bias of induced immune response. The IgG1/IgG2a ratio was calculated after the second booster for each mouse serum. The results for each experimental group (n=6; females) are expressed as means ± SD; $*p \leq 0.01$.

4.14 Molecular Modeling

Ligand and Protein Preparation. Three-dimensional models of compounds were built in ChemBio3D Ultra 16.0.[79] Their geometries were optimized using MMFF94[80] force field and partial atomic charges were added. Energy was minimized until the gradient value was smaller than 0.001 kcal/(mol Å). The optimized structure was further refined with GAMESS interface in ChemBio3D Ultra 16.0 using the semiempirical PM3 method, QA optimization algorithm and Gasteiger Hückel charges for all atoms for 100 steps.[79] Molecular docking calculations were performed using GOLD Suite v5.4,[81,82] running on four octal core AMD Opteron CPU processors, 16 GB RAM, two 750 GB hard drives, running 64-bit Scientific Linux 6.0. Receptor was prepared in a GOLD graphical user interface. Hydrogen atoms were added to the protein and correct tautomers and protonation states were assigned. Water molecules were deleted from the crystal structure. The b*inding site on the concave surface of NOD2 LRR domain was defined by selecting amino acid residues within a radius of 12 Å around Arg857 (PDB entry: 5IRN[51]).

Ligand Docking. Compounds were docked to the defined binding site in 25 independent genetic algorithm (GA) runs by applying different GA parameters (population size = 100,

selection pressure = 1.1, number of operations = 100,000, number of islands = 5, niche size = 2, crossover frequency = 95, mutation frequency = 95, migration frequency = 10) and scoring functions (GoldScore, ChemScore, CHEMPLP). The most representative results were obtained using GoldScore as a scoring function. Ligands with RMSD value less than 1.5 Å were joined in clusters and early termination was allowed if the top 3 solutions were within 1.0 Å of the RMSD value. Proposed binding modes of the top five highest scored docking poses per ligand were evaluated and the highest ranked binding pose was used for graphical representation in PyMOL.[83]

4.15 Screening against PAINS

All tested compounds were screened against the PAINS filter as available in CANVAS (Schrödinger Release 2017-1**:** Canvas, Schrödinger, LLC, New York, NY, 2017). All compounds passed the PAINS filter.

4.16 Liquid Chromatography with tandem Mass spectrometry (LC-MS/MS)

For LC-MS/MS quantitation of compounds 9 and 17 in cell incubation media and lysate samples, an Agilent 1290 Infinity / 6460 Triple Quadrupole detector (Agilent Technologies, Santa Clara, USA) was used. The chromatographic separation was achieved on a Kinetex C18 50 × 2.1 mm, 2.6 µm column (Phenomenex, Torrance, USA) operated at 50 °C and using a gradient elution with a flow rate of 0.65 mL/min and consisted of 0.1% formic acid in water (mobile phase A) and 99.8% acetonitrile (mobile phase B) with the following steps (min, %B): (0.5, 10), (2.5, 18), (3.0-3.5, 82), (3.75, 10). Total run time was 5 min. The injection volume was 1 and 2 µL for the quantification in extracellular medium and cell lysate samples, respectively. Quantification was performed in negative ESI mode using the multiple reaction monitoring with widest (2.5 amu) resolution. The parameters of JetStream® ion source were

as follows: Gas flow (and temperature): 10 L/min (275 °C), Nebulizer pressure: 45 psi, Sheath gas flow (and temperature): 11 L/min (350 °C) and the Capillary voltage was 3500V. For compound **9**, the following m/z transitions were used: 535.3 → 134.5 at 40 eV and 535.3 → 150.6 at 45 eV for quantifier and qualifier ion, respectively. For compound **17**, m/z 479.2 → 128.4 at 35 eV and 479.2 → 111.0 at 25 eV were used for quantifier and qualifier ion, respectively. The retention times of compounds **9** and **17** were 3.53 min and 2.88 min, respectively (Fig. S7). The method was evaluated for selectivity, working range, accuracy, precision and sensitivity (limit of quantification). The method's limit of quantification has been proven to be 0.0625 µM for compounds **9** and **17**, based on the signal/noise ratio criterion of more than 30:1 (Area, Peak-to-Peak) and based on bias of less than ± 20% and precision better than 20% RSD (Fig. S8, Table S5). The calibration lines for compound **9** and compound **17** that cover the concentration range of both analytes from 0.0625 to 4.00 μM are shown in Fig. S9. The results are expressed as means of duplicates ± S.E.M. of two independent experiments measured in two parallels.

4.16.1 Determination of extra- and intracellular concentration. HEK-Blue NOD2 cells (Invivogen, San Diego/CA, USA) were treated with 2 μM of compound **9** or **17** for 18 h. Afterwards, supernatants were collected and cells were lysed in water. The lysates were sonicated, rocked on ice for 30 min and centrifuged at 13,000 rpm at 4 °C for 15 min. Supernatants were collected and stored at -80 °C.The intracellular molarity of compounds **9** and **17** was determined based on the concentration found in the supernatant after centrifugation of methanol-treated cell lysate. The recovery of both compounds from the cell lysate was determined in a separate experiment.

4.16.2 Recovery and matrix effect. The analyte recovery and possible matrix effects were determined by spiking the known amounts of compounds **9** and **17** into blank incubation medium, cell supernatant and cell lysate. After the sample preparation and LC-MS analysis,

the obtained responses were compared to the responses from matrix-free methanolic solution at the same nominal analyte concentration (2 μM) and expressed as percentage (Fig. S10). The values close to 100% show that the method has negligible matrix effects and complete recovery from all the tested media.

4.17 Statistics

In vitro evaluations of cytotoxicity (Fig. S12), NOD2/NOD1 agonistic action (Fig. 2), specificity of compounds (Fig. S13) and dose-dependent NOD2 agonistic action (Fig. 3) were each performed in three independent experiments, with average values expressed as means of duplicates ± S.E.M. (the data was analyzed using descriptive statistics). *In vitro* evaluation of cell uptake and stability (shown in Fig. 4) was performed in two independent experiments, with average values expressed as means of duplicates ± S.E.M. (the data was analyzed using descriptive statistics). *In vitro* experiment on PBMCs (shown in Fig. 6) was performed twice (two independent donors) with average values expressed as means of duplicates ± S.E.M (the data was analyzed using descriptive statistics). Statistical significance was determined by Student t-test (two-tailed; unpaired). Differences were considered significant for $p<0.05$.

The *in vivo* experiment in mice was performed in three experimental groups consisting of 6 female mice (as described in detail in chapter **4.11**). Statistical difference between experimental groups in the production of total anti-OVA IgGs (shown in Fig. 7) was determined by Kruskal–Wallis ANOVA, followed by multiple Mann–Whitney U-nonparametric tests. Differences were considered significant for $p<0.05$. Statistical difference between experimental groups in terms of the anti-OVA IgG1/anti-OVA IgG2a ratio (listed in Table 1) was determined by Kruskal–Wallis ANOVA, followed by multiple Mann–Whitney U-nonparametric tests. The results for each experimental group (n=6; females) are expressed

as means ± SD. Differences were considered highly significant for $p<0.01$. Analyses were performed using Statistica 6.0 for Windows, StatSoft Inc.

ASSOCIATED CONTENT

Supporting Information

The Supporting Information is available free of charge on the ACS Publications website at http://pubs.acs.org/:

Synthesis details for compounds **1a-1c**, **25a-b**, **26a-b**, **27a-b** and analytical data/characterization of intermediate compounds **3a-b**, **18-21**, **25a**, **26a**, **27a**; Supporting Schemes, Figures and Tables; Experimental procedure for Molecular Dynamics Simulation; Experimental procedure for bacterial endotoxin test; 1H and 13C NMR spectra of representative tested compounds (PDF)

Molecular formula strings (CSV)

PDB-ID code of file used for docking experiments: 5IRN (PDB)

AUTHOR INFORMATION

Corresponding author

*Ž.J.: phone 0038614769646; e-mail, ziga.jakopin@ffa.uni-lj.si

ORCID

Žiga Jakopin: 0000-0001-9384-0858

Author Contributions

The study was designed by Ž.J and M.G. The synthetic work was conducted by Ž.J. and M.A. *In vitro* assays of cytotoxicity, NOD1 and NOD2 stimulation, and PBMC isolation and stimulation were conducted by M.G. Characterization of selected compounds, preparation of experimental liposomal formulations and *in vivo* experiments (immunization experiments,

analysis of sera) were conducted by A.Š. and R.F. The *in vitro* stability and cell uptake experiments were conducted by M.G., J.T. and Ž.J. The *in silico* experiments (docking, MD simulation) were conducted by T.T. Ž.J., M.G. and T.T. wrote the manuscript. Ž.J., M.G., T.T., A.Š., R.F., M.A., I.M.R. and J.T. analyzed the data, have read the manuscript and given approval to the final version.

Notes

The authors declare no competing financial interest.

ACKNOWLEDGMENTS

This work was supported by the Slovenian Research Agency grant (No. 0787-P208) and the Croatian Science Foundation (HrZZ) (Project No. 7387). We thank Roger Pain for proofreading the manuscript and Izidor Sosič for meaningful discussions.

ABBREVIATIONS

CARD, caspase activation and recruitment domain; CES, human carboxylesterase; DCC, dicyclohexylcarbodiimide; DMAP, 4-dimethylaminopyridine; EDC, 1-ethyl-3-(3-dimethylaminopropyl)carbodiimide; HOBt, 1-hydroxybenzotriazole; LPS, lipopolysaccharide; LRR, leucine-rich repeats; MAPK, mitogen-activated protein kinase; MDP, muramyl dipeptide; Mur*N*Ac, *N*-acetylmuramyl; NF-κB, nuclear factor κB; NLR, NOD-like receptor; NOD, nucleotide-binding oligomerization domain; OVA, ovalbumin; PBMC, peripheral blood mononuclear cells; PRR, pattern recognition receptors; RIP2, receptor-interacting serine-threonine kinase; SAR, structure/activity relationship; SEAP, secreted embryonic alkaline phosphatase; TLR, toll-like receptor; TFA, trifluoroacetic acid.

5. REFERENCES

[1] Janeway C.A. Jr; Medzhitov R. Innate immune recognition. *Annu. Rev. Immunol.* **2002**, *20*, 197-216.

[2] Philpott, D. J.; Sorbara, M. T.; Robertson, S. J.; Croitoru, K.; Girardin, S. E. NOD proteins: regulators of inflammation in health and disease. *Nat. Rev. Immunol.* **2014**, *14*, 9-23.

[3] Caruso, R.; Warner, N.; Inohara, N.; Nuñez, G. NOD1 and NOD2: signaling, host defense, and inflammatory disease. *Immunity* **2014**, *41*, 898-908.

[4] Proell, M.; Riedl, S. J.; Fritz, J. H.; Rojas, A. M.; Schwarzenbacher, R. The Nod-like receptor (NLR) family: a tale of similarities and differences. *PLoS One* **2008**, *3*, e2119.

[5] Girardin, S. E.; Boneca, I. G.; Viala, J.; Chamaillard, M.; Labigne, A.; Thomas, G.; Philpott, D. J.; Sansonetti, P. J. Nod2 is a general sensor of peptidoglycan through muramyl dipeptide (MDP) detection. *J. Biol. Chem.* **2003**, *278*, 8869-8872.

[6] Inohara, N.; Ogura, Y.; Fontalba, A.; Gutierrez, O.; Pons, F.; Crespo, J.; Fukase, K.; Inamura, S.; Kusumoto, S.; Hashimoto, M.; Foster, S. J.; Moran, A. P.; Fernandez-Luna, J. L.; Nuñez, G. Host recognition of bacterial muramyl dipeptide mediated through NOD2. *J. Biol. Chem.* **2003**, *278*, 5509-5512.

[7] Mo, J.; Boyle, J. P.; Howard, C. B.; Monie, T. P.; Davis, B. K.; Duncan, J. A. Pathogen sensing by nucleotide-binding oligomerization domain-containing protein 2 (NOD2) is mediated by direct binding to muramyl dipeptide and ATP. *J. Biol. Chem.* **2012**, *287*, 23057-23067.

[8] Grimes, C. L.; De Zoysa Ariyananda, L.; Melnyk, J. E.; O'Shea, E. K. The innate immune protein Nod2 binds directly to MDP, a bacterial cell wall fragment. *J. Am. Chem. Soc.* **2012**, *134*, 13535-13537.

[9] Jakopin, Ž. Nucleotide-binding oligomerization domain (NOD) inhibitors: a rational approach toward inhibition of NOD signaling pathway. *J. Med. Chem.* **2014**, *57*, 6897-6918.

[10] Kobayashi, K. S.; Chamaillard, M.; Ogura, Y.; Henegariu, O.; Inohara, N.; Nuñez, G.; Flavell, R. A. Nod2-dependent regulation of innate and adaptive immunity in the intestinal tract. *Science* **2005**, *307*, 731-734.

[11] Magalhaes, J. G.; Fritz, J. H.; Le Bourhis, L.; Sellge, G.; Travassos, L. H.; Selvanantham, T.; Girardin, S. E.; Gommerman, J. L.; Philpott, D. J. Nod2-dependent Th2 polarization of antigen-specific immunity. *J. Immunol.* **2008**, *181*, 7925-7935.

[12] Pavot, V.; Rochereau, N.; Resséquier, J.; Gutjahr, A.; Genin, C.; Tiraby, G.; Perouzel, E.; Lioux, T.; Vernejoul, F.; Verrier, B.; Paul, S. Cutting edge: New chimeric NOD2/TLR2 adjuvant drastically increases vaccine immunogenicity. *J. Immunol.* **2014**, *193*, 5781-5785.

[13] Uehori, J.; Fukase, K.; Akazawa, T.; Uematsu, S.; Akira, S.; Funami, K.; Shingai, M.; Matsumoto, M.; Azuma, I.; Toyoshima, K.; Kusumoto, S.; Seya, T. Dendritic cell maturation induced by muramy dipeptide (MDP) derivatives: monoacylated MDP confers TLR2/TLR4 activation, *J. Immunol.* **2005**, *174*, 7096-7103.

[14] Fritz, J. H.; Girardin, S. E.; Fitting, C.; Werts, C.; Mengin-Lecreulx, D.; Caroff, M.; Cavaillon, J. M.; Philpott, D. J.; Adib-Conguy, M. Synergistic stimulation of human monocytes and dendritic cells by Toll-like receptor 4 and Nod1- and Nod2-activating agonists. *Eur. J. Immunol.* **2005**, *35*, 2459-2470.

[15] Tada, H.; Aiba, S.; Shibata, K.; Ohteki, T.; Takada, H. Synergistic effect of Nod1 and Nod2 agonists with toll-like receptor agonists on human dendritic cells to generate interleukin-12 and T helper type 1 cells. *Infect. Immun.* **2005**, *73*, 7967-7976.

[16] Kleinnijenhuis, J.; Quintin, J.; Preijers, F.; Joosten, L. A. B.; Ifrim, D. C.; Saeed, S.; Jacobs, C.; van Loenhout, J.; de Jong, D.; Stunnenberg, H. G.; Xavier, R. J.; van der Meer, J. W. M.; van Crevel, R.; Netea, M. G. Bacille Calmette-Guérin induces NOD2-dependent nonspecific protection from reinfection via epigenetic reprogramming of monocytes. *PNAS USA* **2012**, *109*, 17537-17542.

[17] van der Meer, J. W. M.; Joosten, L. A. B.; Riksen, N.; Netea, M. G. Trained immunity: a smart way to enhance innate immune defence. *Mol. Immunol.* **2015**, *68*, 40-44.

[18] Geddes, K.; Magalhães, J. G.; Girardin, S. E. Unleashing the therapeutic potential of NOD-like receptors. *Nat. Rev. Drug Disc.* **2009**, *8*, 465-479.

[19] Ellouz, F.; Adam, A.; Ciorbaru, R.; Lederer, E. Minimal requirements for adjuvant activity of bacterial peptidoglycan derivatives. *Biochem. Biophys. Res. Commun.* **1974**, *59*, 1317-1325.

[20] Maisonneuve, C.; Bertholet S.; Philpott, D. J.; De Gregorio, E. Unleashing the potential of NOD- and Toll-like agonists as vaccine adjuvants. *Proc. Natl. Acad. Sci. USA* **2014**, *111*, 12294-12299.

[21] Hancock, R. E. W.; Nijnik, A.; Philpott, D. J. Modulating immunity as a therapy for bacterial infections. *Nat. Rev. Microbiol.* **2012**, *10*, 243-254.

[22] Lefrancier, P.; Lederer, E. Muramyl-peptides. *Pure & Appl. Chem.* **1987**, *59*, 449-454.

[23] Yang, H.-Z.; Xu, S.; Liao, X.-Y.; Zhang, S.-D.; Liang, Z.-L.; Liu, B.-H.; Bai, J.-Y.; Jiang, C.; Ding, J.; Cheng, G.-F.; Liu, G. A novel immunostimulator, N^2-[α-*O*-benzyl-*N*-(acetylmuramyl)-L-alanyl-D-isoglutaminyl]-N^6-*trans*-(*m*-nitrocinnamoyl)-L-lysine, and its adjuvancy on the hepatitis B surface antigen. *J. Med. Chem.* **2005**, *48*, 5112-5122.

[24] Jakopin, Ž.; Corsini, E.; Gobec, M.; Mlinarič-Raščan, I.; Sollner Dolenc, M. Design, synthesis and biological evaluation of novel desmuramyldipeptide analogs. *Eur. J. Med. Chem.* **2011**, *46*, 3762-3777.

[25] Jakopin, Ž.; Gobec, M.; Mlinarič-Raščan, I.; Sollner Dolenc, M. Immunomodulatory properties of novel nucleotide oligomerization domain 2 (Nod2) agonistic desmuramyldipeptides. *J. Med. Chem.* **2012**, *55*, 6478-6488.

[26] Jakopin, Ž. Murabutide revisited: a review of its pleiotropic biological effects. *Curr. Med. Chem.* **2013**, *20*, 2068-2079.

[27] Li, X.; Yu, J.; Xu, S.; Wang, N.; Yang, H.; Yan, Z.; Cheng, G.; Liu, G. Chemical conjugation of muramyl dipeptide and paclitaxel to explore the combination of immunotherapy and chemotherapy for cancer. *Glycoconj. J.* **2008**, *25*, 415-425.

[28] Kikelj, D.; Pečar, S.; Kotnik, V.; Štalc, A.; Wraber-Herzog, B.; Simčič, S.; Ihan, A.; Klamfer, L.; Povšič, L.; Grahek, R.; Suhadolc, E.; Hočevar, M.; Hönig, H.; Rogi-Kohlenprath, R. *N*-{*trans*-[[2'(acetylamino)cyclohexyl]oxy]acetyl}-L-alanyl-D-glutamic acid: a novel immunologically active carbocyclic muramyl dipeptide analogue. *J. Med. Chem.* **1998**, *41*, 530-539.

[29] Sollner, M.; Kotnik, V.; Štalc, A.; Simčič, S.; Povšič, L.; Herzog-Wraber, B.; Klampfer, L.; Ihan, A.; Grosman, P. Apyrogenic synthetic desmuramyldipeptide, LK-409, with immunomodulatory properties, *Agents Actions* **1993**, *38*, 273-280.

[30] Todate, A.; Suda, T.; Kuwata, H.; Chida, K.; Nakamura, H. Muramyl dipeptide-Lys stimulates the function of human dendritic cells. *J. Leukocyte Biol.* **2001**, *70*, 723-729.

[31] Parant, M.A.; Audibert, F.M.; Chedid, L.A.; Level, M.R.; Lefrancier, P.L.; Choay, J.P.; Lederer, E. Immunostimulant activities of a lipophilic muramyl dipeptide derivative and of desmuramyl peptidolipid analogs, *Infect. Immun.* **1980**, *27*, 826-831.

[32] Willems, M. M.; Zom, G. G.; Meeuwenoord, N.; Khan, S.; Ossendorp, F.; Overkleeft, H. S.; van der Marel, G. A.; Filippov, D. V.; Codée, J. D. Lipophilic muramyl dipeptide-antigen conjugates as immunostimulating agents. *ChemMedChem* **2016**, *11*, 190-198.

[33] Zhao, N.; Ma, Y.; Zhang, S.; Fang, X.; Liang, Z.; Liu, G. New muramyl dipeptide (MDP) mimics without the carbohydrate moiety as potential adjuvant candidates for a therapeutic hepatitis B vaccine (HBV). *Bioorg. Med. Chem. Lett.* **2011**, *21*, 4292-4295.

[34] Gobec, M.; Mlinarič-Raščan, I.; Sollner Dolenc, M.; Jakopin, Ž. Structural requirements of acylated Gly-l-Ala-d-Glu analogs for activation of the innate immune receptor NOD2. *Eur. J. Med. Chem.*, **2016**, 116, 1-12.

[35] Sun, D.; Wang, Y.; Tan, F.; Fang, D.; Hu, Y.; Smith, D. E.; Jiang, H. Functional and molecular expression of the proton-coupled oligopeptide transporters in spleen and macrophages from mouse and human. *Mol. Pharmaceutics* **2013**, *10*, 1409-1416.

[36] Nakamura, N.; Lill, J. R.; Phung, Q.; Jiang, Z.; Bakalarski, C.; de Mazière, A.; Klumperman, J.; Schlatter, M.; Delamarre, L.; Mellman, I. Endosomes are specialized platforms for bacterial sensing and NOD2 signalling. *Nature* **2014**, *509*, 240-244.

[37] Lee, J.; Tattoli, I.; Wojtal, K. A.; Vavricka, S. R.; Philpott, D. J.; Girardin, S. E. pH-dependent internalization of muramyl peptides from early endosomes enables Nod1 and Nod2 signaling. *J. Biol. Chem.* **2009**, *284*, 23818–23829.

[38] Marina-García, N.; Franchi, L.; Kim, Y. G.; Hu, Y.; Smith, D. E.; Boons, G. J.; Nuñez, G. Clathrin- and dynamin-dependent endocytic pathway regulates muramyl dipeptide internalization and NOD2 activation. *J. Immunol.* **2009**, *182*, 4321-4327.

[39] Smrdel, P.; Grabnar, I.; Locatelli, I.; Černe, M.; Andrenšek, S.; Kovačič, N.; Kristl, A.; Bogataj, M.; Urleb, U.; Mrhar, A. Physicochemical and preclinical pharmacokinetic and toxicological evaluation of LK-423, a new phthalimido-desmuramyl-dipeptide derivative with immunomodulating activity. *Drug. Dev. Ind. Pharm.* **2009**, *35*, 1293-1304.

[40] Masumoto, J.; Yang, K.; Varambally, S.; Hasegawa, M.; Tomlins, S. A.; Qiu, S.; Fujimoto, Y.; Kawasaki, A.; Foster, S. J.; Horie, Y.; Mak, T. W.; Nuñez, G.; Chinnaiyan, A. M.; Fukase, K.; Inohara, N. Nod1 acts as an intracellular receptor to stimulate chemokine production and neutrophil recruitment in vivo. *J. Exp. Med.* **2006**, *203*, 203-213.

[41] Jakopin, Ž.; Gobec, M.; Kodela, J.; Hazdovac, T.; Mlinarič-Raščan, I.; Sollner Dolenc, M. Synthesis of conformationally constrained γ-D-glutamyl-meso-diaminopimelic acid derivatives as ligands of nucleotide-binding oligomerization domain protein 1 (Nod1). *Eur. J. Med. Chem.* **2013**, *69*, 232-243.

[42] Rubino, S. J.; Magalhaes, J. G.; Philpott, D.; Bahr, G. M.; Blanot, D.; Girardin, S. E. Identification of a synthetic muramyl peptide derivative with enhanced Nod2 stimulatory capacity. *Innate Immun.* **2013**, *19*, 493-503.

[43] Adam, A.; Petit, J.-F.; Lefrancier, P.; Lederer, E. Muramyl peptides. *Mol. Cell. Biochem.* **1981**, *41*, 27-47.

[44] Lefrancier, P.; Derrien, M.; Jamet, X.; Choay, J. Apyrogenic, adjuvant-active N-acetylmuramyl-dipeptides. *J. Med. Chem.* **1982**, *25*, 87-90.

[45] Dinkova-Kostova, A. T.; Abeygunawardana, C.; Talalay, P. Chemoprotective properties of phenylpropenoids, bis(benzylidene)cycloalkanones, and related Michael acceptors: correlation of potencies as phase 2 enzyme inducers and radical scavengers. *J. Med. Chem.* **1998**, *41*, 5287-5296.

[46] Talele, T. T. The »cyclopropyl fragment« is a versatile player that frequently appears in preclinical/clinical drug molecules. *J. Med. Chem.* **2016**, *59*, 8712-8756.

[47] Sosič, I.; Barreteau, H.; Simčič, M.; Šink, R.; Cesar, J.; Zega, A.; Golič Grdadolnik, S.; Contreras-Martel, C.; Dessen, A.; Amoroso, A.; Joris, B.; Blanot, D.; Gobec, S. Second-generation sulfonamide inhibitors of D-glutamic acid-adding enzyme: activitiy optimisation with conformationally rigid analogues of D-glutamic acid. *Eur. J. Med. Chem.* **2011**, *46*, 2880-2894.

[48] Ma, Y.; Zhao, N.; Liu, G. Conjugate (MTC-220) of muramyl dipeptide analogue and paclitaxel prevents both tumor growth and metastasis in mice. *J. Med. Chem.* **2011**, *54*, 2767-2777.

[49] (a) Dong, Y.; Wang, S.; Wang, C.; Li, Z.; Ma, Y.; Liu, G. Antagonizing NOD2 signaling with conjugates of paclitaxel and muramyl dipeptide derivatives sensitizes paclitaxel therapy and significantly prevents tumor metastasis. *J. Med. Chem.* **2017**, *60*, 1219-1224. (b) Wang, S.; Yang, Y.; Li, X.; Liu, Z.; Wu, Y.; Si, G.; Tao, Y.; Zhao, N.; Hu, X.; Ma, Y.; Liu, G.

Discovery of 1,4-benzodiazepine-2,5-dione (BZD) derivatives as dual nucleotide binding oligomerization domain containing 1/2 (NOD1/NOD2) antagonists sensitizing paclitaxel (PTX) to suppress Lewis lung carcinoma (LLC) growth in vivo. *J. Med. Chem.* **2017**, *60*, 5162-5192.

[50] Lauro, M. L.; D'Ambrosio, E. A.; Bahnson, B. J.; Grimes, C. L. Molecular recognition of muramyl dipeptide occurs in the leucine-rich repeat domain of Nod2. *ACS Infect. Dis.* **2017**, *3*, 264-270.

[51] Maekawa, S.; Ohto, U.; Shibata, T.; Miyake, K.; Shimizu, T. Crystal structure of NOD2 and its implications in human disease. *Nat. Commun.* **2016**, *7*, 1111813. doi: 10.1038/ncomms11813.

[52] Rickard, D. J.; Sehon, C. A.; Kasparcova, V.; Kallal, L. A.; Zeng, X.; Montoute, M. N.; Chordia, T.; Poore, D. D.; Li, H.; Eidam, P. M.; Haile, P. A.; Yu, J.; Emery, J. G.; Marquis, R. W.; Gough, P. J.; Bertin, J. Identification of benzimidazole diamides as selective inhibitors of the nucleotide-binding oligomerization domain 2 (NOD2) signaling pathway. *PLoS One* **2013**, *8*, e69619.

[53] Merhi, G.; Coleman, A.W.; Devissaguet, J.-P.; Barratt, G.M. Synthesis and immunostimulating properties of lipophilic ester and ether muramyl peptide derivatives, *J. Med. Chem.* **1996**, *39*, 4483-4488.

[54] Jakopin, Ž. The design and synthesis of Ala-Glu/iGln mimetics: heterocyclic building blocks for pseudopeptides. *Tetrahedron Lett.* **2015**, *56*, 504-506.

[55] Markey, G. M. Carboxylesterase 1 (Ces1): from monocyte marker to major player. *J. Clin. Pathol.* **2011**, *64*, 107-109.

[56] Allen Crow, J.; Herring, K. L.; Xie, S.; Borazjani, A.; Potter, P. M.; Ross, M. K. Inhibition of carboxylesterase activity of THP1 monocytes/macrophages and recombinant

human carboxylesterase 1 by oxysterols and fatty acids. *Biochim. Biophys. Acta* **2010**, *1801*, 31-41.

[57] Chanteux, H.; Rosa, M.; Delatour, C.; Prakash, C.; Smith, S.; Nicolas, J.-M. In vitro hydrolysis and transesterification of CDP323, an α4β1/α4β7 integrin antagonist ester prodrug. *Drug Metab. Disp.* **2014**, *42*, 153-161.

[58] Thomsen, R.; Rasmussen, H. B.; Linnet, K.; the INDICES Consortium. In vitro drug metabolism by human carboxylesterase 1: focus on angiotensin-converting enzyme inhibitors. *Drug Metab. Disp.* **2014**, *42*, 126-133.

[59] Imai, T.; Taketani, M.; Shii, M.; Hosokawa, M.; Chiba, K. Substrate specificity of carboxylesterase isozymes and their contribution to hydrolase activity in human liver and small intestine. *Drug Metab. Disp.* **2006**, *34*, 1734-1741.

[60] Xie, M.; Yang, D.; Liu, L.; Xue, B.; Yan, B. Human and rodent carboxylesterases: immunorelatedness, overlapping substrate specificity, differential sensitivity to serine enzyme inhibitors, and tumor-related expression. *Drug Metab. Disp.* **2002**, *30*, 541-547.

[61] Pratt, S. E.; Durland-Busbice, S.; Shepard, R. L.; Heinz-Taheny, K.; Iversen, P. W.; Dantzig, A. H. Human carboxylesterase-2 hydrolyzes the prodrug of gemcitabine (LY2334737) and confers prodrug sensitivity to cancer cells. *Clin. Cancer. Res.* **2013**, *19*, 1159-1168.

[62] Maharana, J.; Patra, M. C.; De, C. D.; Sahoo, B. R.; Behera, B. K.; De, S.; Pradhan, S. K. Structural insights into the MDP binding and CARD-CARD interaction in zebrafish (*Danio rerio*) NOD2: a molecular dynamics approach. *J. Mol. Recognit.* **2014**, *27*, 260-275.

[63] Asensio, J. L.; Ardá, A.; Cañada, F. J.; Jiménez-Barbero, J. Carbohydrate-aromatic interactions. *Acc. Chem. Res.* **2013**, *46*, 946-954.

[64] Hudson, K. L.; Bartlett, G. J.; Diehl, R. C.; Agirre, J.; Gallagher, T.; Kiessling, L. L.; Woolfson, D. N. Carbohydrate-aromatic interactions in proteins. *J. Am. Chem. Soc.* **2015**, *137*, 15152-15160.

[65] Goodchild, A.; Nopper, N.; Craddock, A.; Law, T.; King, A.; Fanning, G.; Rivory, L.; Passioura, T. Primary leukocyte screens for innate agonists. *J. Biomol. Screening* **2009**, *14*, 723-730.

[66] Rostaing, L.; Tkaczuk, J.; Durand, M.; Peres, C.; Durand, D.; de Préval, C.; Ohayon, E.; Abbal, M. Kinetics of intracytoplasmic Th1 and Th2 cytokine production assessed by flow cytometry following in vitro activation of peripheral blood mononuclear cells. *Cytometry* **1999**, *35*, 318-328.

[67] Pauleau, A.-L.; Murray, P.J. Role of Nod2 in the response of macrophages to Toll-like receptor agonists. *Mol. Cell. Biol.* **2003**, *23*, 7531-7539.

[68] van der Meer, J. H. M.; Netea, M. G.; Dinarello, C. A. Modulation of muramyl dipeptide stimulation of cytokine production by blood components. *Clin. Exp. Immunol.* **2009**, *156*, 428-433.

[69] Traub, S.; von Aulock, S.; Hartung, T.; Hermann, C. MDP and other muropeptides – direct and synergistic effects on the immune system. *J. Endotoxin Res.* **2006**, *12*, 69-85.

[70] Tukhvatulin, A. I.; Dzharullaeva, A. S.; Tukhvatulina, N. M.; Shcheblyakov, D. V.; Shmarov, M. M.; Dolzhikova, I. V.; Stanhope-Baker, P.; Naroditsky, B. S.; Gudkov, A. V.; Logunov, D. Y.; Gintsburg, A. L. Powerful complex immunoadjuvant based on synergistic effect of combined TLR4 and NOD2 activation significantly enhances magnitude of humoral and cellular adaptive immune responses. *PLoS One* **2016**, 11(5): e0155650. doi: 10.1371/journal.pone.0155650.

[71] (a) Turánek, J.; Mašek, J.; Raška, M.; Ledvina, M. Application of liposomes for construction of vaccines. In *Biomedical Science, Engineering and Technology*; Ghista, D. N.,

Ed.; InTech, 2012; pp 653-678. (b) Effenberg, R.; Knötigova, P.T.; Zyka, D.; Čelechovská, H.; Mašek, J.; Bartheldyová, E.; Hubatka, F.; Koudelka, Š.; Lukáč, R.; Kovalová, A.; Šaman, D.; Křupka, M.; Barkocziova, L.; Kosztyu, P.; Šebela, M.; Drož, L.; Hučko, M.; Kanásová, M.; Miller, A.D.; Raška, M.; Ledvina, M.; Turánek, J. Nonpyrogenic molecular adjuvants based on norAbu-muramyldipeptide and norAbu-glucosaminyl muramyldipeptide: synthesis, molecular mechanisms of action, and biological activities in vitro and in vivo. *J. Med. Chem.* **2017**, *60*, 7745-7763.

[72] Alving, C.R. Liposomes as as carriers of antigens and adjuvants. *J. Immunol. Meth*. **1991**, *140*, 1-13.

[73] Habjanec, L.; Halassy, B.; Tomašić, J. Comparative study of structurally related peptidoglycan monomer and muramyl dipeptide on humoral IgG response to ovalbumin in mice. *Int. Immunopharmacol.* **2010**, *10*, 751-759.

[74] Habjanec, L.; Frkanec, R.; Halassy, B.; Tomašić, J. Effect of liposomal formulations and immunostimulating peptidoglycan monomer (PGM) on the immune reaction to ovalbumin in mice. *J. Liposome Res.,* **2006**, *16*, 1-16.

[75] Gupta, R. K.; Relyveld, E. H.; Lindblad, E. B.; Bizzini, B.; Ben-Efraim, S.; Gupta, C. K. Adjuvants – a balance between toxicity and adjuvanticity. *Vaccine* **1993**, *11*, 293-306.

[76] Frkanec, R.; Travaš, D.; Krstanović, M.; Halassy Špoljar, B.; Ljevaković, Đ.; Vranešić, B.; Frkanec, L.; Tomašić, J. Entrapment of peptidoglycans and adamantyltripeptides into liposomes: an HPLC assay for determination of encapsulation efficiency. *J. Liposome Res*. **2003**, *13*, 279-296.

[77] Frkanec, R.; Noethig Laslo, V.; Vranešić, B.; Mirosavljević, K.; Tomašić, J. A spin labelling study of immunomodulating peptidoglycan monomer and adamantyltripeptides entrapped into liposomes. *Biochim. Biophys. Acta,* **2003**, *1611*, 187-196.

[78] Halassy, B.; Krstanović, M.; Frkanec, R.; Tomašić, J. Adjuvant activity of peptidoglycan monomer and its metabolic products, *Vaccine,* **2003**, 21, 971-976.

[79] GAMESS interface, ChemBio3D Ultra 13.0, ChemBioOffice Ultra 13.0, CambridgeSoft.

[80] Halgren, T. A. Merck molecular force field .1. Basis, form, scope, parameterization, and performance of MMFF94. *J. Comput. Chem.* **1996**, *17*, 490-519.

[81] Jones, G.; Willett, P.; Glen, R. C.; Leach, A. R.; Taylor, R. Development and validation of a genetic algorithm for flexible docking. *J. Mol. Biol.* **1997**, *267*, 727–748.

[82] GOLD Suite v5.4 is available from The Cambridge Crystallographic Data Centre, 12 Union Road, Cambridge, CB2 1EZ, UK, www.ccdc.cam.ac.uk.

[83] PyMOL, Delano Scientific LLC, San Francisco, CA, http://pymol.sourceforge.net.

TABLE OF CONTENTS GRAPHIC